A THESIS SUBMITTED TO
THE GRADUATE SCHOOL OF NATURAL AND APPLIED SCIENCES
OF ÇANKIRI KARATEKİN UNIVERSITY

PRODUCTION AND CHARACTERIZATION OF HETEROSTRUCTURED NiO/FTO-NiO/ITO-NiO/GLASS FILMS

IN PARTIAL FULFILLMENT OF THE REQUIREMENTS
FOR
THE DEGREE OF MASTER OF SCIENCE
IN
PHYSICS

BY

AHMED MAJEED FADHIL ALSAMARAI

ÇANKIRI

2023

PRODUCTION AND CHARACTERIZATION OF HETEROSTRUCTURED NiO/FTO-NiO/ITO-NiO/GLASS FILMS

By Ahmed MAJEED FADHIL ALSAMARAI

April 2023

We certify that we have read this thesis and that in our opinion it is fully adequate, in scope and in quality, as a thesis for the degree of Master of Science

Advisor **:** Assoc. Prof. Dr. Olcay GENÇYILMAZ

Examining Committee Members:

Chairman **:** Assoc. Prof. Dr. Olcay GENÇYILMAZ
Material and Material Processing Technologies
Çankırı Karatekin University

Member **:** Asst. Prof. Dr. İlker KARA
Department of Medical Services and Techniques
Çankırı Karatekin University

Member **:** Asst. Prof. Dr. Emrah SARICA
Electric Electronic Engineering
Başkent University

Approved for the Graduate School of Natural and Applied Sciences

Prof. Dr. Hamit ALYAR
Director of Graduate School

I hereby declare that all information in this document has been obtained and presented in accordance with academic rules and ethical conduct. I also declare that, as required by these rules and conduct, I have fully cited and referenced all material and results that are not original to this work.

Ahmed MAJEED FADHIL ALSAMARAI

ABSTRACT

PRODUCTION AND CHARACTERIZATION OF HETEROSTRUCTURED NiO/FTO-NiO/ITO-NiO/GLASS FILMS

Ahmed MAJEED FADHIL ALSAMARAI

Master of Science in Physics

Advisor: Assoc. Prof. Dr. Olcay GENÇYILMAZ

April 2023

In this thesis, nickel oxide (NiO) films were produced using different substrates using the cascading ion layer adsorption and reaction (SILAR) method. NiO films were deposited on Glass, FTO and ITO substrates, and NiO/FTO, NiO/ITO, and NiO/Glass films were obtained. Structural, optical, electrical, and surface properties of the produced films were investigated. In addition, the effect of the used substrates on the physical properties of NiO films was investigated. By using X-ray patterns, the structural properties of the films such as crystallization level, grain size, micro-strain, unit cell constants and dislocation density were determined. All films have a cubic crystal structure and a preferential orientation in the (200) direction, and the grain sizes of the films range from 30-60 nm. As a result of the optical analyzes of the films, it was determined that the optical energy range values changed in the range of 3.56-4 eV. In addition, it was determined that the use of ITO base significantly increased the permeability values (~40 %). The electrical properties of the films were investigated by current-voltage (I-V) characterization. All films have ohmic electrical properties. The ideal factor (η) and voltage barrier (ϕ_B) values of the films changed in the range of 1.44-3.44 and 0.49-0.59 eV, respectively. By examining the surface morphologies of the films, it was determined that they have a homogeneous distribution and the choice of substrate affects the grain size on the surface.

2022, 76 pages

Keywords: NiO film, Glass, Fto, Ito, Heterostructure, Sılar method

ÖZET

HETERO YAPILI NiO/FTO-NiO/ITO-NiO/CAM FİLMLERİNİN ÜRETİM VE KARAKTERİZASYONU

Ahmed MAJEED FADHIL ALSAMARAI
Fizik, Yüksek Lisans
Tez Danışmanı: Doç. Dr. Olcay GENÇYILMAZ
Nisan 2023

Bu tez çalışmasında, Sıralı İyon Adsorpsiyon ve Reaksiyon yöntemi (SILAR) ile farklı tabanlar kullanılarak nikel oksit (NiO) filmlerinin üretimi ve karakterizasyonu yapılmıştır. NiO filmlerinin üretiminde Glass, FTO, ITO olmak üzere üç farklı taban kullanılarak NiO-Glass, NiO-FTO, NiO-ITO filmleri elde edilmiştir. Üretilen filmlerin yapısal, optiksel, elektriksel ve yüzeysel özellikleri incelenmiştir. Ayrıca kullanılan tabanların NiO filmlerinin fiziksel özellikleri üzerine etkisi araştırılmıştır. X-ışını desenleri kullanılarak filmlerin kristalleşme seviyesi, tane boyutu, mikro gerilme, birim hücre sabitleri ve dislokasyon yoğunluğu gibi yapısal özellikleri belirlenmiştir. Tüm filmler kübik bir kristal yapıda ve (200) doğrultusunda tercihli bir yönelime sahiptir ve tane boyutları 30-60 nm arasında değişmektedir. Filmlerin optik analizleri sonucu, optik enerji aralığı değerlerinin 3,56 – 4 eV aralığında değiştiği tespit edilmiştir. Ayrıca ITO taban kullanımının geçirgenlik değerlerini (~% 40) belirgin bir şekilde arttırdığı belirlenmiştir. Filmlerin elektriksel özellikleri akım-voltaj (I-V) karakterizasyonu yapılarak incelenmiştir. Tüm filmler omik elektriksel özelliğe sahiptir. Filmlerin ideal faktör (η) ve voltaj bariyeri (ϕ_B) değerleri sırasıyla 1,44-3,44 ve 0,49-0,59 eV aralığında değiştirmiştir. Filmlerin yüzey morfolojileri incelenerek homojen bir dağılıma sahip olduğu ve taban seçiminin yüzeydeki tane boyutunu etkilediği tespit edilmiştir.

2023, 76 sayfa

Anahtar Kelimeler: NiO filmi, Cam, Fto, Ito, Heteroyapı, Sılar yöntemi

PREFACE AND ACKNOWLEDGEMENTS

Greetings of pride and thanks to our wonderful supervisor for her sincere efforts with me throughout the days of study, Dr. Olcay Gençyılmaz. All due respect and appreciation to Dr. İlker Kara for his wonderful advice and guidance.

Many thanks to the state of Turkey, which took it upon itself to spread science and civilization in the country.

Thanks and appreciation to Çankırı Karatekin University and the Department of Physics for their organization and great effort.

Thanks and appreciation to all my loved ones and family for their support and help.
Thanks and appreciation to my colleagues at University, especially my best friend (Berkan Hafizoğlu) who helped me every step of the way.

Ahmed MAJEED FADHIL ALSAMARAI
Çankırı-2023

CONTENTS

LIST OF SYMBOLS

B	A constant that depends on the nature of the substance
A	Absorption (%)
α	Absorption coefficient (cm^{-1})
NH_3	Ammonia
n	An exponential constant whose value depends on the nature of the transitions
Å	Angstrom unit
ϕ_B	Barrier height (eV)
h	Blank's constant (6.636×10^{-34} joul.sec)
K_b	Boltzmanne constant 1.338×10^{-23} joul. K^{-1}
n*	Complex refractive
BC	Conduction band (eV)
I	Current (Amp)
J	Current density (Amp/cm^2)
I-V	Current voltage technique
k	Damping coefficient (cm^{-1})
n	Density of charge carriers ($1/cm^3$)
θ_B	Diffraction angle
δ	Dislocation density ($Lines/nm^2$)
m*	Effective mass (kg)
eV	Elctron volt
q	Electron charge (1.6×10^{-19} Coulomb)
σ	Electrical conductivity $(\Omega.cm)^{-1}$
E	Electric field (volt/cm)
ρ	Electrical resistivity (Ω.cm)
E_g	Energy gap (eV)
ν	Frequency (1/sec)
G	Grain size (nm)
η	Ideality factor
i	Imaginary number
I_0	Intensity of incoming light
I_A	Intensity of light absorbed
I_R	Intensity of the light reflected
K	Kilven
a°	Lattice constant (Å)
d_{hkl}	Lattice dimensions (Å)
ε	Micro strain
hkl	Miller's indices
Ni^{+2}	Nickel ion

$NiCl_2$	Nickel(II) chloride
Ω	Ohm
σ°	Optical conductivity (1/sec)
O^-	Oxygen ion
$ø_{TC}$	Quality factor (Ω^{-1})
%	Percent
ε_1	Real part of the dielectric constant
R	Reflectance (%)
n°	Refractive index
τ	Relaxation time (sec)
A*	Richardson constant: (27-32 $A.K^{-2}$ cm^2)
R_S	Surface resistance (Ω)
Δm	The difference in substrate weight (mg)
$I_{(hkl)}$	The measured intensity of the level (hkl)
$I_{0(hkl)}$	The standard intensity of the level (hkl) taken from the (JCPDS) card
V	The voltage (Volt)
d	Thin thickness
T	Transmittance (%)
I	Transmitted light intensity
E_u	Urbach energy (eV)
k	Wave vector (1/nm)
λ	Wavelength (nm)

LIST OF ABBREVIATIONS

CVD	Chemical Vapor Deposition
FCC	Face Centered Cubic
FTO	Fluorine doped tin oxide
FWHM	Full width at half maximum curve
Sol-Gel	Gel solution method
ITO	Indium doped tin oxide
NiO	Nickel oxide
NiO-FTO	Nickel oxide films deposited on glass fluorine doped tin oxide substrates
NiO-Glass	Nickel oxide films deposited on glass substrates
NiO-ITO	Nickel oxide films deposited on glass indium doped tin oxide substrates
PVD	Physical vapor deposition
SILAR	Successive ionic layer adsorption and reaction
TC(hkl)	Texture coefficient
JCPDS	The international card for measurements
TCO	Translucent conductive oxides
UV	Ultraviolet
VIS	Visible ray
XRD	X-ray diffraction

LIST OF FIGURES

LIST OF TABLES

1. INTRODUCTION

Semiconductor thin films are an important class of materials used in various electronic devices. These films, typically just a few nanometers to microns thick, are deposited on a substrate through techniques such as chemical vapor deposition or sputtering (Hedges and Oades 1997). They possess unique electrical and optical properties, making them ideal for use in appications such as photovolatics, transistors, and sensors. The properties of these films can be tailored by adjusting their composition and thickness, enabling precise control over their performance (Novoselov and Castra 2012). The development of thin film technology has revolutionized the electronics industry, enabling the creation of smaller, faster, and more energy efficient devices (Qu *et al*. 2000).

In a semiconductor, the band energy gap (E_g) is the energy range between the valence band and the conduction band, where no electrons are allowed to exist. This band gap plays a crucial role in many electronic devices (Kalyani and Dhoble 2012 The band energy gap is expressed as the shortest vertical distance between the lowest point of the conduction band and the peak of the valence band. It is also known as the energy required for electrons to move from the valence band to the conduction band. This band gap is called band because there are almost no energy levels (Zhang *et al*. 1998). If the band gap is small, the semiconductor behaves like a metal. If the bandgap is large, the semiconductor behaves like an insulator (Young 2008).

Pure semiconductors have limited electrical conductivity, which is not suitable for most electronic applications. In order to overcome this limitation, semiconductors are doped by forign elements. Doping is the intentional introduction of impurities into a semiconductor material, such as silicon or germanium, in order to modify its electrical properties (Elsheikh *et al*. 2014). A band gap diagram for conductors (metals), semiconductors and insulators is given in Figure 1.1.

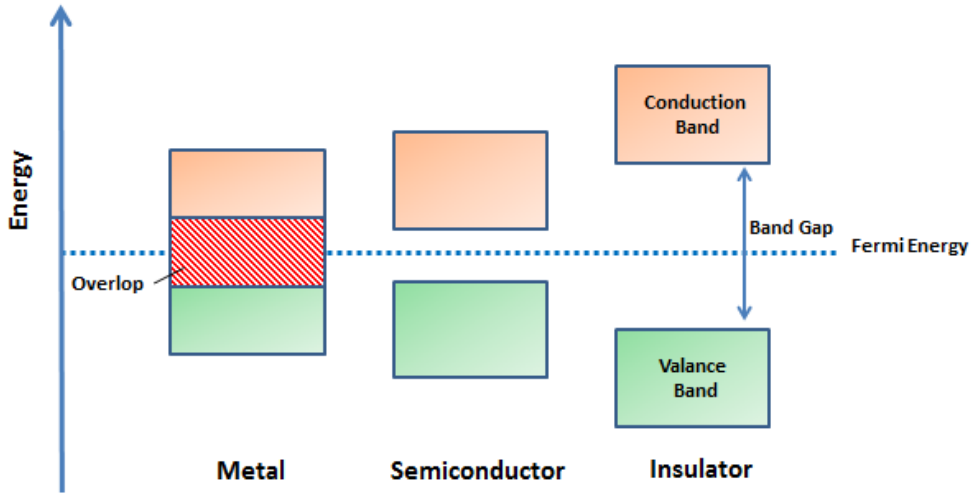

Figure 1.1 A band gap diagram for conductors (metals), semiconductors, and insulators

1.1 Intrinsinc and Doped Semiconductors

Intrinsic semiconductors are pure semiconducting materials, such as silicon (Si) or germanium (Ge), which have no intentional impurities added to them. They have a small but finite conductivity at room temperature (Sze 1981).

Doped semiconductors are materials that have impurities intentionally added to them during the manufacturing process. The impurities, called dopants, can either add extra electrons to the semiconductor material (n-type doping) or create "holes" where electrons are missing (p-type doping). The n-type and p-type semiconductors are created by doping with different elements, such as phosphorus or boron, respectively (Kittel 2004).

1.1.1 n-type semiconductors

n-type semiconductor materials are a type of semiconductor that contains impurities or dopants that introduce free electrons into the semiconductor's conduction band. Phosphorus, arsenic and antimony are often used as doping atoms in N-type

semiconductors. These atoms have an excess of electrons in their outermost shell, unlike the semiconductor material. When these dopants are added to the semiconductor material, they replace some of the original atoms, and the extra electron from the dopant is loosely bound to the atom, allowing it to move freely within the material's crystal lattice. This extra electron is known as a donor electron and is responsible for the n-type conductivity of the material (Gross and Roppel 1996). Therefore, n-type semiconductors have a negative charge carrier concentration, as they have more free electrons than holes (Qu *et al.* 2000, Elkaiem 2015). These free electrons can move freely throughout the material and conduct electricity, making n-type semiconductors useful in electronic devices such as transistors, solar cells, and LEDs.

When a donor atom is introduced into the lattice, they led to creation of donor energy levels in forbidden bandgap and these donor energy levels are typically located near the conduction band of the semiconductor, but slightly below it. This means that the energy required to excite an electron from the donor level to the conduction band is relatively small, allowing the donor electrons to participate in conduction at room temperature (Macdonald 1953).

If the donor level is too deep, the energy required to excite an electron to the conduction band may be too high, leading to a lower concentration of free electrons and reduced conductivity (Raebiger 2007). On the other hand, if the donor level is too shallow, the donor electrons may be easily excited to the conduction band at room temperature (Elsheikh *et al*. 2014).

1.1.2 p-type semiconductors

p-type semiconductor materials are a type of semiconductor that contains impurities, also known as dopants, that increase the number of holes (positively charged vacancies) in the semiconductor crystal lattice. These dopants are typically elements from group III of the periodic table, such as boron, aluminum, or gallium. When a small amount of dopant is added to a semiconductor crystal, it replaces some of the

atoms in the crystal lattice, creating an imbalance in the number of electrons and holes. In p-type semiconductors, the dopant atoms have fewer valence electrons than the atoms they replace, so they create "holes" in the crystal lattice where electrons are missing (Kittel 2004).

The acceptor impurities introduce energy levels in the band gap of the semiconductor, which are referred to as acceptor energy levels. These energy levels are located just above the valence band maximum and are shallow, meaning that they require relatively little energy to ionize and release an electron into the conduction band.

p-type semiconductors are widely used in electronic devices, such as diodes and transistors, because they are capable of conducting electricity in a controlled manner. For example, p-type semiconductors can be used to create p-n junctions, which are important in the construction of diodes and solar cells (Banerjee and Chattopadhyay 2005, Hiramatsu *et al.* 2010, Zakutayev *et al.* 2010).

1.2 Transparent Conductive Oxides (TCOs)

Transparent Conductive Oxides (TCOs) are materials that possess the unique property of being both transparent and conductive. They are widely used in a variety of applications, such as touch screens, solar cells, flat panel displays, and light-emitting diodes (LEDs) (Exarhos and Zhou 2007). The transparency of TCOs is due to their low absorption of light in the visible region of the electromagnetic spectrum. The optical properties of TCOs can be adjusted by controlling their composition, thickness, and surface morphology, allowing for a wide range of applications (Søndergaard *et al*. 2013).

TCOs have two properties not found in other materials. These features are high electrical conductivity and high transmittance. Therefore, TCOs have contributed to developments in the opto-electronics industry and are used in many applications (Exarhos and Zhou 2007). Especially NiO, ZnO, TiO, SnO, MgO and CuO etc. Oxide

semiconductors such as photodetector, sensor, photodiode, solar cell are among the most used materials in applications (Caporaletti 1982).

In addition to their use in electronic devices, TCOs have also been investigated for their potential in other areas, such as sensing, catalysis, and energy storage (Caporaletti 1982). For example, TCOs have been used as gas sensors to detect harmful gases, such as carbon monoxide, and as catalysts in the conversion of carbon dioxide to fuels.

1.2.1 ITO thin films

Tin-doped indium oxide (ITO), a highly degenerate n-type semiconductor. It is among the TCOs due to its superior optical and electrical properties over other materials. Today, ITO is mainly used in the opto-electronics industry, with applications such as liquid crystal displays, light-emitting diodes, solar cells, gas sensor and touch screens due to its high conductivity, excellent transparency and chemical stability (Vander Kam *et al.* 1999, Sauter *et al.* 2000, Beyer *et al.* 2007). However, ITO is expensive and contains rare elements, such as indium, which limits its use in large-scale applications (Granqvist and Hultåker 2002).

ITO thin films have a face-centered cubic (FCC) crystalline structure and their optical bandgap is in the range of 3.2 to 4.0 eV, depending on the deposition conditions (Antony *et al.* 2004). This wide bandgap allows for good visible light transmission while blocking UV radiation, making it useful for applications that require transparent conductors (Pissadakis *et al.* 1999).

1.2.2 FTO thin films

FTO (Fluorine-doped Tin Oxide) thin films are a type of transparent conductive oxide film that has obtained very attention in recent years. FTO thin films are made up of a crystalline structure of tin oxide that has been doped with fluorine atoms. The anionic

radius of F^- (1.33Å) is similar to that of the O^{2-} atom (1.32Å). Therefore, F doping is used to reduce the distortions caused by other doping atoms in the lattice. Thus, FTO films with the same crystal structure as SnO_2 are obtained. The crystal structure of FTO films is known as rutile with tetragonal unit cells (Zhang 2017).

The addition of fluorine atoms to the tin oxide lattice results in a decrease in the material's electrical resistivity and an increase in its transparency in the visible region of the electromagnetic spectrum (Wu *et al.* 2010). This unique combination of properties makes them an ideal material for use as a transparent electrode (Noh *et al.* 2012). FTO thin films are abundant in nature, and the primary raw materials used for their synthesis (tin and fluorine) are relatively inexpensive and widely available. This abundance and low cost have made them a popular choice for industrial applications.

The optical bandgap of FTO thin films is typically in the range of 3.4-4.0 eV, which makes them transparent in the visible region of the electromagnetic spectrum. This transparency, combined with their excellent electrical conductivity, makes them an ideal material for use in optoelectronic devices, such as transparent electrodes in solar cells and displays (Hudaya *et al.* 2015, Batzill and Diebold 2005, Dauzhenka *et al.* 2011).

1.2.3 Comparison betweeen (ITO) and (FTO) substrates

Tin-doped Indium Oxide (In_2O_3:Sn) and Fluorine-doped Tin Oxide (SnO_2:F) films are transparent conductive materials obtained by these methods and ITO and are called FTO. Although they have a lower conductivity than ITO films, FTO films are preferred over ITO films due to their high heat resistance and chemical stability (Kalelei *et al.* 2019). ITO and FTO films have wide band gap ($\geq$3 eV) and show n-type semiconductor properties (Colombel *et al.* 2009, Moholkar 2007). Also, in the visible spectrum region, ITO and FTO films are frequently used in optoelectronic devices because of the good compatibility between optical transmittance and electrical conductivity (Kim *et al.* 2006, Elangovan *et al.* 2005).

Despite the optical superiority of glass (ITO) substrates, (FTO) substrates have higher thermal tolerance without change in resistivity value. This is useful for increasing the efficiency of some devices that require a higher annealing temperature than (ITO) (Li *et al.* 2014). The adsorption of (ITO) substrates differs from (FTO) substrates and depends on the interaction of precipitants with these substrates. In addition, the size of the particles formed causes an increase in scattering and reflection and a decrease in absorption at some wavelengths (Abuelwafa *et al.* 2021b). (ITO) substrates have greater permeability than visible range (FTO) substrates due to the surface roughness of (FTO) (Aouaj *et al.* 2009). FTO films have higher efficiency in some photovoltaic cells and are used as electrodes. It can also be used instead of high-cost ITO films (Hu et al. 2011).

1.2.4 NiO thin films

Nickel oxide (NiO) is a semiconductor known as (Bunsénite) classified as conductive metal oxide (Chavillon 2011). Its molecular formula (NiO) is in the form of green or black crystalline powder (Chang et al. 1998), with density (6.67 g/cm3) and molecular weight (842.87 g/mol). Its sources are nitrate, chloride, and acetate. It dissolves in alcohol and other solutions, so the solution becomes dark green, and has a wide direct band gap (3.6 eV-4 eV) with positive electrical conductivity (p-type). Nickel oxide is a chemically stable material with outstanding electrical and optical properties. It is a magnetic material, that is, it has important magnetic properties, low preparation cost, and good durability (Patil and Kadam 2002).

NiO is an abundant transition metal oxide that has attracted considerable attention in the field of thin-film technology due to its unique electronic and optical properties (Napari *et al*. 2021). NiO have a rock salt structure with a cubic lattice, where Ni ions occupy the face-centered cubic lattice and oxygen ions occupy the octahedral sites. The lattice parameter of the NiO crystal structure is around 4.18 Å. Nickel oxide is a chemical compound with the formula NiO. It has a face-centered cubic crystal structure (FCC) in Figure 1.2. It is similar in structure to sodium chloride (NaCl). Because the Na^{2+} and Cl^{-} ions in the NaCl structure are similar to the nickel Ni^{+2} ions

and oxygen O^{-2} ions in the NiO structure. It has a space group (Fm-3m) and a lattice constant (a=4.1769 nm) (Diao *et al*. 2020).

The locations of the oxygen ions are at the vertices of the cube and the centers of the faces, while the locations of the nickel ions are at the center of the cube and the middle of the sides of the cube. The place that the oxygen atom resides in (0.5, 0, 0) and the nickel atom occupies the position (0,0,0) and the level (100). It is a common plane consisting of 50 % (Ni) and (50 %) of (O), while the (111) plane is alternately. The face (111) is polar and therefore unstable, opposite to (100), which is considered non-polar, so it is stable (Smart and Moore 2012). The value of the ionic radius for nickel and oxygen is:

$$R\ (Ni^{+2}) = 0.72\ Å \quad (1.1)$$

$$R\ (O^{-2}) = 1.40\ Å \quad (1.2)$$

Nickel oxide is a p-type semiconductor, also an antiferromagnetic, and a substance that changes color when an electric field is applied to it. It is one of the most important electronic materials after tungsten oxide (Chavillon 2011). Table 1.1 shows some electrical properties of nickel oxide films.

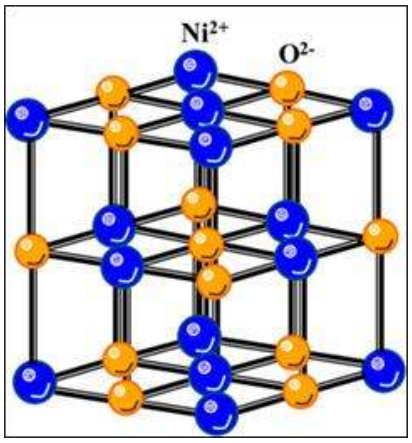

Figure 1.2 The locations of the Nickel and Oxygen ions in the crystal lattice

NiO has a wide optical band gap of around 3.6 eV, which corresponds to a wavelength of 344 nm. This wide band gap makes NiO transparent in the visible region of the electromagnetic spectrum and opaque in the ultraviolet region. This property makes it a suitable candidate for applications in transparent conductive electrodes, solar cells, and optoelectronic devices. In addition, NiO thin films have also been studied for their gas sensing properties. NiO has been also shown to exhibit high sensitivity towards gases such as NO_2 and CO, making it a potential candidate for gas sensor applications.

Table 1.1 Some electrical properties of nickel oxide

PROPERTIES	**VALUES**
Conductivity (σ)	10 (1/Ω.cm)
Mobility (μ)	0.1–1 (cm /V.sec)
Density of charge carriers (n)	10^{18} –10^{19} (1/cm^3)
Energy gap (E_g)	3.6–4 eV
Dielectric constant (ε)	11.9

Nickel oxide is a semiconductor and is transparent to ultraviolet, visible and near infrared rays (Benzarouk 2008). As for the transparency of nickel oxide in the visible range, it is related to valency and the value of the refractive index (n) is approximately in the range (1.6-2.33) and the transmittance takes the value (40-80 %) (Abu Yaqoub 2012).

Nickel oxide (NiO) has a wide direct energy gap in the range (3.6- 4 eV), the energy gap of nickel oxide varies with the different deposition methods used, and Figure 1.3 shows a diagram of the structure of energy levels for nickel oxide (Barir 2018). Also, the values of some properties of nickel oxide are given in Table 1.2.

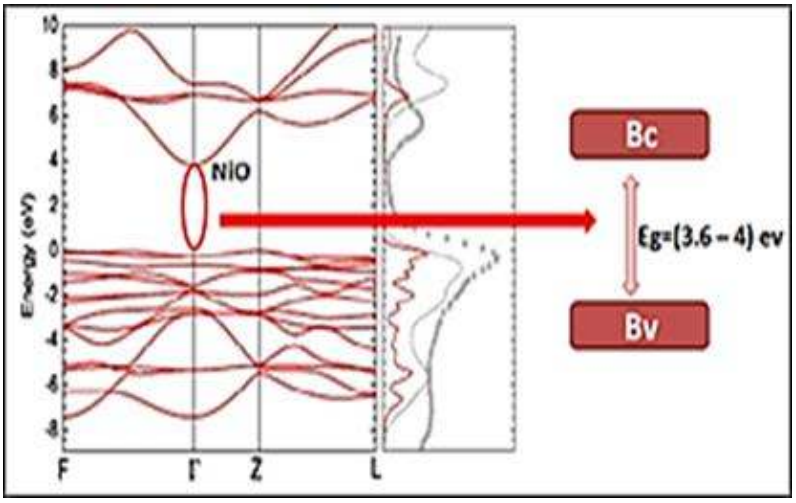

Figure 1.3 The energy gap of nickel oxide (NiO) (Barir 2018)

Table 1.2 The values of some properties of nickel oxide

CHEMICAL FORMULA	**NiO**
Molar mass	842.87 gm/mol
Density	6.67 g/cm^3
Crystal structure	Face-Centered Cubic (FCC)
Space group	Fm-3m
Crystal lattice constants	a=b=c= 4.1769 Å
Energy gap (E_g)	3.6 – 4 eV
Color	green or black
Refractive index	1.6-2.33
Transmittance (T)	(40-80 %)

2. LITERATURE REVIEW

2.1 Literature Review TCOs

Transparent conductive oxides (TCO) were discovered in 1907 by Karl Baedeker by discovering cadmium oxide (CdO) in the form of thin films, which he considered a transparent conductive oxide with a low band gap and low light transparency (Khalifa 2015). The first use of transparent conducting oxides was after the discovery of indium oxide doped with tin ($Sn:In_2O_3$) in 1954 by (Rupprecht and Güler 2020). In 1960, binary compounds such as In_2O_3, SnO_2, and ZnO appeared (Ellmer and Klein 2008), and it was discovered that they are good transparent conducting oxides. After 1980, tenary compounds appeared, such as $CdIn_2O_4$, as well as multiple compounds (Nazarzadehmoafi 2017) and in most of the transparent conducting oxides, most of them were n-type semiconductor. The p- type TCO was observed in 1993 by the researcher H. Sato with his co-workers represented in nickel oxide in which the majority of the charge carriers are the holes, and since 1995 TCO have attracted great interest on the part of researchers to study it in the form of thin slices and in recent years the publication of scientific articles on this subject has increased significantly (Sullivan *et al*. 2016).

Transparent Conducting oxides have many advantages that made them of great importance in scientific applications (Hecht *et al*. 2011), including:

- Electrical conductivity increases with increasing temperature, and this property is one of the properties that distinguish it from other conductive materials.
- Semiconductors have a high sensitivity that may lead to an increase in conductivity when they contain impurities or defects, and it can also result in one type of charge carrier, which means a decrease or disappearance of the other type.
- High electrical conductivity and transparency at visible wavelengths (400-800 nm).

- The conduction band is full of free electrons and has high conductivity and optical transmittance.
- The Fermi level is very close to the conduction band.

Transparent conductive oxides have important electrical and optical properties. These properties have led researchers to develop and benefit from them due to their high light transparency, good electrical conductivity and applicability in different technologies (Lopez 2003). Since 1970, interest has begun to study the electrical properties of transparent conductive oxides. These oxides have more usage areas compared to other semiconductors, especially due to their excellent electrical properties (Padvi *et al*. 2021).

In 2007, information is given about the discovery of TCO materials, their electrical and optical properties. Types of TCO materials, production techniques and application areas are explained. Information about materials which are alternative to TCO materials is also given (Clark 2007).

In 2007, A review attempt has been made about TCO movies. In this study, general load carrier mechanisms, production techniques and carrier mobility of TCOs are given. The features that TCOs should have according to their usage areas are explained (Exarhos and Zhou 2007).

In 2007, The efficiency in photovoltaic (PV) devices where transparent conductive oxides (TCOs) act as electrode elements, structural templates, and diffusion barriers and where their operating function controls the open-circuit device voltage has been determined. The TCO properties and processing matrix as TCOs are applied to current and future PV technologies are studied (Fortunato *et al.* 2007).

In 2015, electrode applications of TCO materials and some physical properties of alternative TCO materials that can be used in these applications have been studied (Minami 2005).

In 2018, applications of TCO materials in the production of transparent electrodes, especially for optoelectronic device applications, are described. The latest developments about TCO and TCO types are mentioned. The properties of different types of TCO materials were compared. In addition, he was able to talk about the properties and usage areas of doped TCOs (Afre *et al.* 2018).

In 2019, the physical mechanisms and derived applications of TCO-based thin-film devices are discussed in terms of how to deliberately exploit their optical properties associated with oxygen defects under illumination, such as PPC. For photo-sensing applications, it has been found that a positive voltage pulse is required to get rid of the PPC after illumination (Jang *et al.* 2019).

In 2023, based on a review of ongoing research and development, this article discusses the deposition of TCO films by various techniques, the parameters affecting TCO properties, the properties of doped and undoped TCO materials and their effects on SHJ SC efficiency (Chavan *et al.* 2023).

2.2 Literature Review ITO and FTO Films

ITO (indium tin oxide) and FTO (fluorine doped tin oxide) films are the typical most widely used transparent conductive oxides (TCO) substrates. Both films are used in optoelectronic devices such as inorganic solar cells, organic solar cells and dye-sensitized solar cells, panel displays and sensors.

Indium tin oxide (ITO) films are prepared as an inorganic mixture of indium (III) oxide (In_2O_3) and tin (IV) oxide (SnO_2). It can be produced as powder and thin film. Indium Tin Oxide (ITO) is formed by the reaction between tin oxide and indium oxide. While its color changes from yellow to gray in powder form, it has a transparent appearance when produced as a thin film. Therefore, it is among the materials used as a transparent thin film. ITO is an n-type degenerate semiconductor and a good conductive. ITO films are generally coated on glass due to their low cost.

In addition, glass is a low-resistance and transparent material. ITO films are often used in electronic and opto-electronic applications. It is frequently used especially in optical coating, hot mirrors and beam splitter applications.

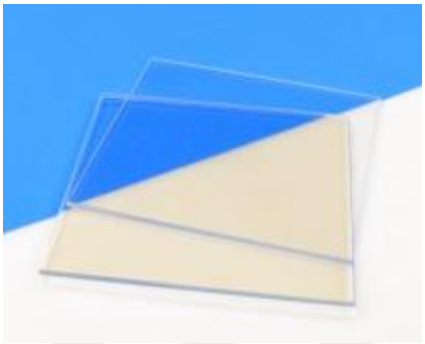

Figure 2.1 Photograph of indium tin oxide (ITO) (NTFL Your Coating Solution 2023)

Fluorine doped tin oxide (FTO) is obtained by adding fluorine to tin oxide. FTO films are high trasparent and low resistance materials in polycrystal structure. FTO is an attractive n-type wide band gap semiconductor. The photographs of ITO and FTO films are shown in Figure 2.1 and Figure 2.2, respectively.

Figure 2.2 Photograph of fluorine doped tin oxide (FTO) (Biotain 2023)

Both ITO and FTO films belong to the TCO family. However, while ITO films are produced as compounds, FTO films are obtained by doping. This situation causes both films to have different physical and chemical properties. FTO films can be used at higher temperatures than ITO films. FTO can be used up to 600 °C, while ITO films are used up to 300 °C.

In 2003, ITO and FTO films were produced at 350 °C and 400 °C using chemical spraying technique, respectively. These films were defined as new transparent conductive oxide films. It has been shown that the lowest electrical resistivity is 1.4×10^{-4} Ωcm and its transmittance is 80 % higher (Kawashima *et al.* 2003).

In 2009, ITO and FTO films were produced using chemical spraying technique at 400 °C. Some physical features of the films were compared. It has been shown that ITO and FTO films with high optical transparency and conductivity can be produced simply and economically. Their electrical resistivities were found on the order of 10^{-4} Ωcm (Aouaj *et al.* 2009).

In 2011, ITO and FTO films were deposited on soda-lime glass substrates at 300 °C using radio frequency magnetron sputtering method, and the photovoltaic performances of the films were investigated. The photoconversion efficiency (η) of dye-sensitized solar cell (DSC) films using ITO was 5.64%, while it was 2.73% and 6.47% for DSC films with ITO and FTO, respectively (Kwak *et al.* 2011).

In 2013, the effect of potentiodynamic stress on the structural and morphological properties of FTO and ITO commercial materials was investigated. The electrochemical behaviors of films were determined. The main results were that the structural and morphological properties of FTO substrates after cathodic polarization remained almost constant compared to ITO films (Plá Cid *et al.* 2013).

In 2017, a review study was conducted on the medical, food and environmental applications of indium tin oxide (ITO) films. Especially the latest developments in

biosensor and sensor applications of ITO films are explained (Aydın and Sezgintürk 2017).

In 2020, the effects of annealing on the physical properties of ITO, FTO and TiO_2 films were investigated. As a result of annealing, it was determined that the electrical and optical properties of the FTO films improved, while the ITO films got worse. In addition, it has been determined that TiO_2 films have the highest photoconversion efficiency in annealing in oxygen environment (Nguyen *et al.* 2020).

In 2022, metal electrodes have been investigated as an alternative to ITO and FTO films used in conventional dye-sensitized solar cells. Unlike FTO and ITO, flexible metal electrodes have been proposed for dye-sensitized solar cells. The effects of different electrode materials were compared by testing the current-voltage characteristics (Yang *et al.* 2022).

In 2023, FTO and ITO films have been produced for flexible perovskite solar cells. In addition, the roughness effects of the films were investigated. It has been shown that it is possible to switch from a conventional but rough FTO that is not compatible with a flexible substrate to a flat ITO (Holzhey *et al.* 2023).

2.3 Literature Review NiO-ITO and NiO-FTO Films

In 2008, Electrochromic properties, structure and surface properties of NiO films coated with sol-gel technique on ITO substrate were investigated. The properties of films coated with both spinning and dipping techniques were compared (Zayim *et. al* 2008).

In 2015, NiO films were produced on FTO substrate by sol-gel spin coating technique. The produced films were annealed in air, oxygen, nitrogen and argon environments. The effect of annealing medium on the structural, morphological, optical and electrochemical properties of NiO-FTO films was investigated. From the FESEM

results, the films are compact, dense and well adhered to the surfaces and have a smooth, homogeneous surface morphology. FESEM images of NiO films annealed in air and oxygen medium have been found to have almost the same surface morphology as films annealed in inert medium. It has been found that NiO films annealed under oxygen in air and atmosphere show high transmittance, whereas there is a corresponding decrease in the transmittance of films annealed in other medium. Cyclic voltammetry results showed that anodic peak shift occurred for films annealed in argon and nitrogen (Taşköprü 2016).

In 2019, NiO films in nanosheet structure were produced on the ITO substrates by using the solution immersion method. Production was made at different growing times and the effect of growing time was examined. In this study, it has been shown that the produced NiO nanolayer films have high potential for sensor applications (Abdullah *et. al* 2019).

In 2020, NiO and NiO/WO_3 films were produced on ITO and flexible PEDOT:PSS/Ag/PET substrates using the sol-gel technique. The EC performance and stability of NiO flexible devices are tested using WO_3 as a counter electrode (Rakibuddin *et. al* 2020).

In 2020, NiO films were produced on FTO bases by doping with Sr element at different doping ratios. The opto-nonlinear applications of the films were examined and the effect of Sr contribution on some physical properties was determined (Manthrammel *et. al* 2020).

In 2021, photodetector in p-NiO/Ag/n-ITO heterostructure was produced with RF magnetron sputtering technique for opto-electronic applications. The photodetector properties of the p-NiO/Ag/n-ITO heterostructure were investigated and their applicability was optimized (Ferhati *et. al* 2021).

In 2022, ITO/Metal/NiO sandwich structure was produced by vacuum spraying and thermal evaporation method. In addition, the optical and electrical properties of the transparent conductive oxide structure were investigated. In addition, the structure is doped with metal doping atoms such as Au, Ag, and Cu. The effects of additive atoms on the structure were determined (Ghasemi *et al.* 2022).

3. MATERIAL AND METHOD

Deposition and characterization of thin film semiconductors have tremendous technological and scientific importance in various fields, including electronics, optoelectronics, energy, and materials science. Therefore, in this section, information about thin film deposition techniques and analysis methods is given.

3.1 Deposition Techniques

Transparent thin film deposition techniques refer to a group of processes used to produce a layer of material that is only a few nanometers to several micrometers thick on a substrate surface. Thin films find applications in a variety of fields, such as electronics, optoelectronics, solar cells, fuel cells, coatings, and medical implants. There are several methods for depositing thin films, each with its advantages and disadvantages. Here are some of the commonly used techniques:

Physical Vapor Deposition (PVD): PVD techniques involve the evaporation or sputtering of the material from a target onto the substrate. The most common PVD techniques include thermal evaporation, electron beam evaporation, and magnetron sputtering. These techniques are widely used to deposit metals, alloys, and some ceramics (Frey and Khan 2015, Pulker 2019).

Chemical Vapor Deposition (CVD): CVD is a process that involves the chemical reaction of precursor gases to deposit thin films. The most commonly used CVD techniques include thermal CVD, plasma-enhanced CVD (PECVD), and atomic layer deposition (ALD). CVD is widely used to deposit metals, semiconductors, and insulators (Frey and Khan 2015).

Spin Coating: It is a technique used widely in thin film production. The prepared solution is dripped onto the rotating base at high speeds. The centripetal force and surface tension of the dripping liquid together ensure an even distribution of the

solution on the surface. Thus, the surface is coated. After the remaining solution evaporates, it condenses and turns into a thin film. Spin coating is a simple and inexpensive technique used to deposit thin films on flat substrates. The material is dispensed onto the substrate, which is then spun at high speed to spread the material evenly. Spin coating is widely used to deposit polymers, oxides, and nanoparticles (Birnie 2004).

Spray Pyrolysis: Spray pyrolysis is a technique that involves spraying a solution of the precursor onto a heated substrate. T In this process, the reagents are dissolved in a liquid in the form of tiny droplets and are sprayed onto a hot surface. The solvent evaporates, leaving a thin film of the material. Spray pyrolysis is used to deposit oxide and metal films (Geremew 2022).

Laser Ablation: Laser ablation is a process that involves irradiating a target material with a laser beam to vaporize it. The vaporized material then condenses on the substrate, forming a thin film. Laser ablation is widely used to deposit metals and ceramics (Yang 2017).

Successive Ionic Layer Adsorption and Reaction (SILAR): It involves the alternating immersion of the substrate in two or more solutions, resulting in the formation of layers through ionic adsorption and subsequent chemical reaction (Nicolau 1985).

3.1.1 Successive ionic layer adsorption and reaction (SILAR) technique

Successive Ionic Layer Adsorption and Reaction (SILAR) is a simple and cost-effective technique for depositing thin films of various materials, including semiconductors, metals, and oxides. It was first introduced by D. Tenne and his colleagues in 1986 (Nicolau 1985). The SILAR technique involves the alternate immersion of a substrate into two or more solutions of precursors, where each immersion leads to the deposition of a thin layer of the material onto the substrate surface. During each immersion step, the substrate surface undergoes ionic adsorption

of the precursor ions from the solution, followed by a chemical reaction that leads to the formation of the material layer. The substrate is then washed with a suitable solvent to remove any unreacted precursors and dried before the next immersion step (Figure 3.1).

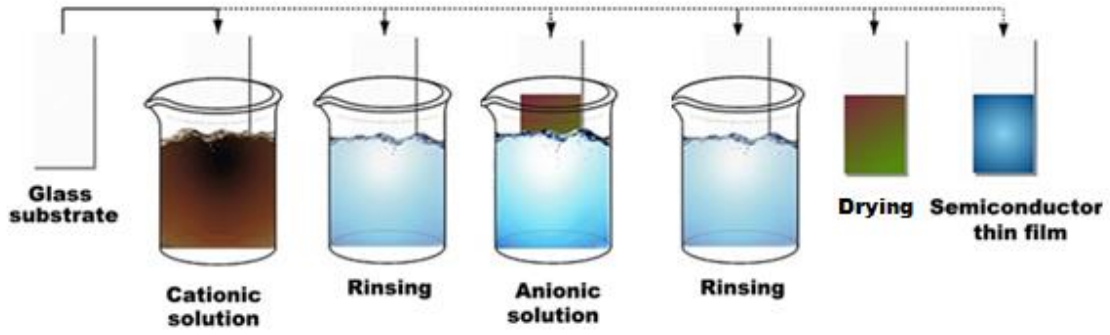

Figure 3.1 Diagram representing the steps of sedimentation by the SILAR method

The SILAR technique offers several advantages over other thin film deposition methods, such as (Nicolau 1985, Pathan and Lokhande 2004):

1. Low cost: SILAR does not require expensive equipment or complex process control systems, making it a cost-effective technique for depositing thin films.
2. Conformal deposition: SILAR can achieve uniform and conformal deposition of materials on complex substrate surfaces, including porous or irregular surfaces.
3. Precise control over thickness: The thickness of the deposited layers can be easily controlled by adjusting the immersion time, the concentration of the precursor solutions, and the number of immersion cycles.
4. Versatility: SILAR can deposit a wide range of materials, including semiconductors and oxides, making it a versatile technique for various applications.

The SILAR technique has been widely used in various fields, including photovoltaics, sensors, catalysis, and corrosion protection. However, SILAR has some limitations, such as a low deposition rate, making it unsuitable for large-scale production (Liu *et al.* 2017). Nevertheless, it remains a valuable technique for producing thin films with specific properties that cannot be achieved using other methods.

3.2 Characterization Techniques

Thin films' properties, such as electrical conductivity, optical transparency, and mechanical strength, depend on their thickness, composition, structure, and morphology (Adachi and Wasa 2012). Therefore, it is crucial to characterize thin films to understand their properties and optimize their performance. Thin film characterizations include X-ray diffraction (XRD), scanning electron microscopy (SEM), transmission electron microscopy (TEM), and atomic force microscopy (AFM). XRD can reveal the crystal structure, lattice parameters, and orientation of thin films, while SEM, TEM, and AFM provide information about the film's morphology, such as surface roughness, grain size, and texture. On the other hand optical spectroscopy, such as UV-Vis absorption and fluorescence, can determine the film's optical properties, such as bandgap and refractive index while electrical measurements, such as resistivity and conductivity, can reveal the film's electrical properties (Yaseen 2012).

3.2.1 Structural characterization

X-ray diffraction (XRD) is a powerful analytical technique that provides information about the crystal structure of materials. It is widely used in materials science, chemistry, physics, and geology to determine the crystal structure, lattice parameters, and orientation of crystalline materials. The technique works by analyzing the diffraction pattern of X-rays that are scattered from the crystal lattice of a sample.

The XRD instrument consists of an X-ray source, a sample holder, a detector, and a computer. The X-ray source emits a beam of X-rays, which is collimated and directed onto the sample. The X-rays interact with the electrons in the crystal lattice, causing them to scatter in different directions (Figure 3.2). The scattered X-rays form a diffraction pattern, which is collected by the detector and analyzed by the computer. The diffraction pattern contains a series of peaks, each of which corresponds to a specific set of crystal planes in the sample. The position and intensity of the peaks provide information about the crystal structure and orientation of the sample.

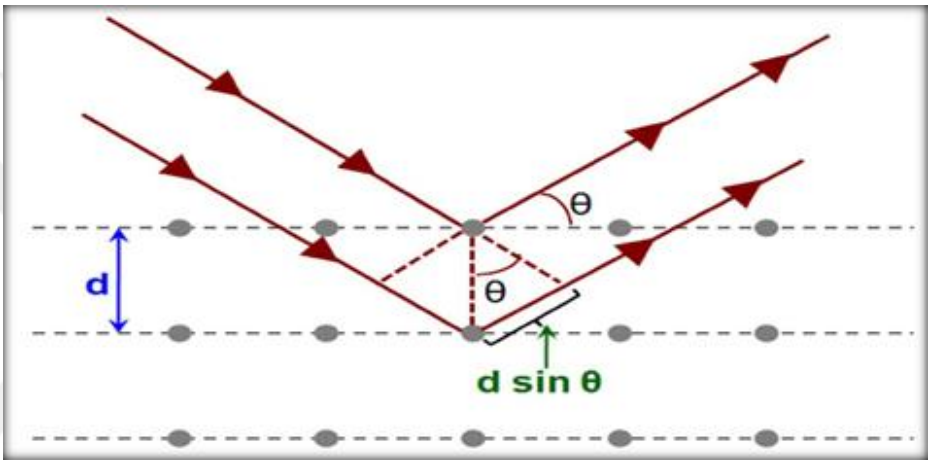

Figure 3.2 The diffraction of X-rays (Baskaran 2010)

The peak position is related to the spacing between the crystal planes, known as the d-spacing, and is given by Bragg's law (Cole 2004):

$$n\lambda = 2d \sin\theta \quad (3.1)$$

where n is an integer, λ is the wavelength of the X-rays, θ is the diffraction angle, and d is the d-spacing of the crystal planes also know as interplanar spacing. The information obtained from Bragg's law includes the lattice parameters, the crystal symmetry, the spacing between the planes of atoms, and the orientation of the crystal with respect to the X-ray beam (Chatterjee 2008). This information is essential for understanding the properties and behavior of materials, including their mechanical,

optical, and electrical properties. An XRD pattern may contain more than one diffraction peaks belongin to different crystal orientations. Therefore, texture coefficient which is a measure of the degree of preferred orientation (texture) of the crystalline grains in a material is calculated. It is commonly used in X-ray diffraction (XRD) analysis to quantify the extent of crystallographic texture in polycrystalline materials. The texture coefficient (TC) is calculated by comparing the intensity of a particular diffraction peak (corresponding to a specific crystallographic plane) in the measured XRD pattern to the intensity that would be expected. The textrure coeffiecent gives Equation (3.2):

$$TC(hkl) = \frac{I_{(hkl)} / I_{0(hkl)}}{N^{-1} \sum_N I_{(hkl)} / I_{0(hkl)}} \quad (3.2)$$

where I_{hkl} is the integrated intensity of the diffraction peak corresponding to the (hkl) plane, N is the number of the diffraction peaks, I_{0hkl} is the standard intensity of the level (hkl) taken from the (JCPDS) card.

Onthe other hand, when the interplanar spacing are obtained with the help of XRD patterns, the lattice parameter of a cubic structure can be found with the following Equation (3.3).

$$d_{hkl} = \frac{a}{\sqrt{h^2+k^2+l^2}} \quad (3.3)$$

where h, k, and l are the Miller indices of the diffraction peak. Additionally, based on the full width at half maximum (FWHM) of a diffraction peak in X-ray diffraction (XRD) data, the average crystallite size (D) in a thin film can be estiamted by means of the Scherrer equation given as follow Equation (3.4).

$$D = \frac{0.9\,\lambda}{\beta \cos\theta} \quad (3.4)$$

where D is the average crystallite size, λ is the wavelength of the X-rays, β is the FWHM of the peak in radians, and θ is the Bragg angle (Dickinson and Cheremisinoff 1980).

Due to the presence of misaligned regions or slip planes in the lattice, dislocations which are defects in the crystal structure of a material may arise and the dislocation density is defined as the measure of the number of dislocation lines per unit area. They can be calculated by following Equation (3.5) (Abed *et al.* 2014):

$$\delta = \frac{1}{D^2} \tag{3.5}$$

Lattice strain refers to the deformation or distortion of the crystal lattice of a material caused by the presence of defects or stresses, such as dislocations or external forces. This lattice strain (ε) can be quantified using following Equation (3.6):

$$\varepsilon = \frac{\beta \cos \theta}{4} \tag{3.6}$$

β is the FWHM of the peak in radians, and θ is the Bragg angle (Abed *et al.* 2014).

3.2.2 Morphological characterization

The surface properties of the films have a significant impact on various physical properties such as their optical and electrical properties. In particular, changes at the joint interface between two or more thin film layers, created by sequential growth, determine the performance of the devices produced (Geremew 2022). Therefore, it is necessary to examine the surface properties of semiconductor thin films using appropriate experimental methods. High-resolution techniques used for this purpose can be classified into two groups: scanning probe microscopy and electron microscopy (Kohli 2012).

The scanning electron microscope (SEM) is one of the most preferred techniques for imaging thin film surfaces. It provides data on the surface topography of materials at a resolution of a few nanometers and enables the collection of information about the elemental composition of the material. To obtain an enlarged image of the sample using SEM, the sample surface is bombarded with a high-energy electron beam and secondary electrons or backscattered electrons released from the sample are detected. SEM devices are also equipped with energy-dispersive X-ray detectors (EDX). By detecting characteristic X-rays emitted from the sample surface using an EDX detector, information can be obtained about the elemental composition of the material. This technique is known as energy-dispersive X-ray spectroscopy (Jaya 2020) .

3.2.3 Optical characterization

Studying the interaction of semiconductor materials with electromagnetic waves plays an important role in determining their physical properties and investigating their usability in optoelectronic devices. When an electromagnetic wave is incident on any material, some materials behaves opaque while others behaves transparent or reflectors.

The transmission (*T*), reflection (*R*), and absorption (*A*) of an occur as a result of interaction material with electromagnetic wave. The total of the reflected, absorbed, and transmitted rates of an electromagnetic wave at a specific wavelength is equal to 1 (Pankove and Carlson 1976). According to Equation (3.7):

$$A + R + T = 1 \tag{3.7}$$

As light travels through a material, some of the light is absorbed by the material, and a decrease in the intensity of the incoming light is observed depending on the path it takes through the material. If the intensity of the incoming light is I_0 and the intensity of the light passing through the material is I, then the relationship between these two quantities is as follows Equation (3.8):

$$\frac{I}{I_0} = e^{-\alpha d} \tag{3.8}$$

where, d refers to the thickness of the material and α is referred to as the linear absorption coefficient. The absorption coefficient can be calculated using the Beer-Lambert formula, depending on the optical absorption and material thickness, with the following Equation (3.9) (Bushberg and Boone 2011).

$$\alpha = 2{,}303\left(\frac{A}{d}\right) \tag{3.9}$$

When photons pass through a material, they lose some of their energy. As a result, the speed of the beam of light decreases and it undergoes refraction. The ratio of the speed of light in a vacuum to the speed of light in the material is defined as the refractive index (n) of the material (Sokolik *et al*. 1993). The general recractive index formula gives Equation (3.10):

$$n = \frac{c}{v} \tag{3.10}$$

Here, c is the speed of light in vacuum and v is the speed it has within the material. The complex refractive index for a semiconductor material is defined Equation (3.11) (Sokolik *et al*. 1993):

$$n = n_0 - ik \tag{3.11}$$

Here, the first term is the real part of the refractive index n_0 given by the Equation (3.12):

$$n_0 = \frac{1+R}{1-R} + \sqrt{\frac{4R}{(1-R)^2} - k^2} \tag{3.12}$$

and the second term represents the imaginary part of the refractive index given by the Equation (3.13):

$$k = \frac{\alpha\lambda}{4\pi} \tag{3.13}$$

where, k is the extinction coefficient (Sokolik *et al*. 1993) .

When photons with a certain frequency (ν) are incident on a pure semiconductor material, if the energy of the photon ($h\nu$) is equal to or greater than the semiconductor material's bandgap energy (E_g), the electrons in the valence band are excited to the conduction band and absorption occurs. This type of absorption is called fundamental absorption.

$$h\upsilon \geq E_g \tag{3.14}$$

Acoording to Equation (3.14), there are two different types of transitions that can be observed in the fundamental absorption region, namely direct and indirect. Materials that have the minimum point of the conduction band and the maximum point of the valence band at the same k value in energy-momentum space are called direct bandgap materials and these materials have direct band transitions (Rahal 2013).

The rapid increase in absorption starts when the energy of the indicent light is approximately equal to the energy gap. The fundamental absorption edge represents the lowest energy difference between the highest point in the valence band and the lowest point in the conduction band (Hamilton 2003).

On the other hand, in indirect bandgap materials, the maximum of the valence band and the minimum of the conduction band are not located at the same k value. In this case, the processes of spontaneously absorption or emission of a phonon take place during excitation of an electron.

There are two types of electronic transition in a semiconductor, the direct and indirect transition, depending on the location of the highest point in the valence band, and the lowest point at the bottom of the conduction band.

This type of electronic transition occurs in semiconductors when the bottom of the conduction beam is in the curve drawn between energy and wave number (E-K) just above the top of the valence band, that is, they have the same wave vector value ($\Delta k = 0$), in this case, it appears absorption when $h\nu = E_g^{opt.}$, this type occurs without a noticeable change in momentum, and there are two types of direct transitions are (Hamilton 2003):

1-The occurrence of the transition between the highest points in the equivalence beam and the lowest point in the conduction beam, and is called direct allowed transition, as in Figure 2.7 case (a) and Figure 2.7 for case (b). The absorption coefficient for this type of transition can be calculated from the relationship Equation (3.15).

$$\alpha h\nu = B(h\nu - E_g^{opt})^n \qquad (3.15)$$

$E_g^{opt.}$ is energy gap (eV), B is A constant that depends on the nature of the substance, h is Plank's constant equal to (6.625 x 10^{-34} J.sec), ν is the frequency of the incident photon (1/sec), n is an exponential constant whose value depends on the nature of the transitions. If (n =1/2) the transition is direct and allowed, and if it is (n = 3/2), the transition is direct and band, α is absorption coefficient (Al-Jawad *et al.* 2016).

In this transition type, the bottom of the conduction band in the (E-K) curve is not completely above the top of the valence band. Therefore, the transfer of electrons from the valence band to the conduction band occurs non-vertical. The value of the electron wave vector is unequal before and after the transition. So ($\Delta k \neq 0$) such phonon assisted transition occurs to conserve momentum caused by the electron's wave vector. Direct and indirect transition types are shown in Figure 3.3. Indirect transfers are of two types:

1- When the transitions are between the highest point in the valence beam and the lowest point in the conduction beam located in different regions of (*k*) space, it is called the permissible indirect transition as in Figure 3.3 case (c).
2- When the transition is between adjacent points to the highest and lowest point in the valence band and the conduction band, it is called a band indirect transition.

The absorption coefficient for this type of transition can be obtained from the following Equation (3.16) (Fallah *et al*. 2007).

$$\alpha h\nu = B(h\nu - E_g^{opt} E_p)^n \qquad (3.16)$$

E_g^{opt}: Energy gap for indirect transmission

n: equals 2 in the case of permissible indirect transfers

n: equals 3 in the case of prohibited indirect transfers

E_P: Auxiliary phonon energy, when (+): phonon absorption, (-): phonon emission (Kasap 2006).

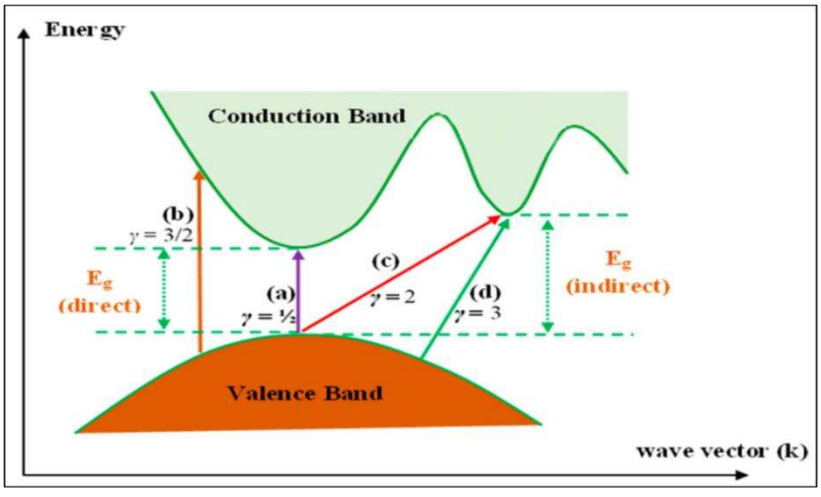

Figure 3.3 Types of transitions (a) direct allowed, (b) direct band, (c) indirect allowed and (d) indirect band (Balestrieri 2014)

In the vicinity of absorption edge, the absorption coefficient (αhv) can be expressed by the following Equation (3.17).

$$(\alpha h\nu) = A(h\nu - E_g)^n \tag{3.17}$$

where *A* is a constant that depends on the effective mass of electrons and holes, as well as the refractive index of the material. The value of *n* is 1/2 for allowed direct transitions, 3/2 for forbidden direct transitions, and 2 for indirect transitions (Al-Jawad *et al.* 2016).

Using an optical method, the energy band gap of a semiconductor material with a direct band gap can be determined by utilizing the absorption spectrum and identifying the point at which the linear portion of the $(\alpha hv)^2$ vs. hv curve intersects the hν axis. In theory, when photons with sufficient energy are absorbed, a sharp increase in the absorption edge is expected to be observed in the absorption spectrum as a result of transitions from the valence band to the conduction band. However, in practice, fluctuations occur at the energy band edge due to factors such as crystal defects or impurities. These fluctuations, called the Urbach tail, cause the absorption edge to increase exponentially. The change in the linear absorption coefficient with respect to photon energy is given by the following equation, known as the Urbach rule. The rule gives Equation (3.18):

$$\alpha(h\nu) = \alpha_0 exp\left(\frac{E-E_g}{E_0}\right) \tag{3.18}$$

Here, E_0 is referred to as the Urbach parameter and is experimentally calculated using the slope of the linear portion of the $ln(\alpha)$ vs. hv plot (Gençyılmaz 2021).

3.2.4 Electrical characterization

The current density ($J=I/A$) resulting from the motion of free carriers under an electric field (E) in semiconductors is given by the following Equation (3.19).

$$J = \sigma E \tag{3.19}$$

where σ represents electrical conductivity (Waremra and Betaubun 2018).

In a semiconductor, electrons and holes contribute to electrical conduction. Therefore, the conductivity is given by the following Equation (3.20).

$$\sigma = n_h q \mu_h + n_e q \mu_e \tag{3.20}$$

where, n_h is the hole concentration, n_e is the electron concentration, μ_h is the hole mobility and μ_e electron mobility (Berg and Purcell 1977). The relationship between conductivity and resistivity (ρ) is as follows Equation (3.21):

$$\rho = \frac{1}{\sigma} = \frac{1}{n_h q \mu_h + n_B q \mu_B} \tag{3.21}$$

The electrical conductivity of a semiconductor material can be determined experimentally using two-point probe, four-point probe, and Van der Pauw methods. The method based on determining the electrical conductivity and specific resistance of the semiconductor material using a simple setup consisting of a voltage source and an ammeter connected to the material through metal contacts is called the two-point probe technique (Figure 3.4 (a)) (Miccoli *et al.* 2015).

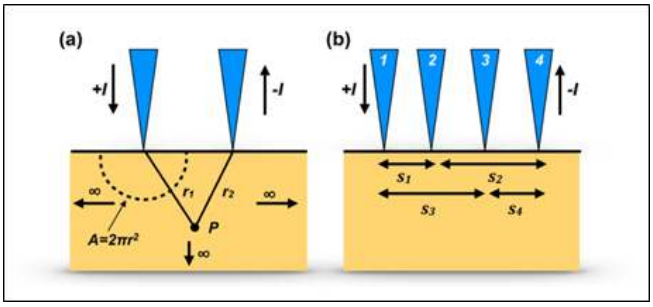

Figure 3.4 Schematic diagram of (a) a two-point probe and (b) collinear four-point probe electric measurement techniques (Miccoli *et al.* 2015)

In the two-point technique, each metal contact is used as both the current and voltage terminals. The current values are measured in response to the applied voltage between the metal contacts, and the slope of the resulting current-voltage (I-V) graph is used to determine the electrical resistance of the material using the following Equation (3.22).

$$\rho = \frac{\Delta V}{\Delta I}\frac{(d \times l)}{L} \tag{3.22}$$

where ρ is the electrical resistance of the material, d is the thickness of the material, L is the distance between the metal contacts, and l represents the length of the contacts (Mesrouk 2013).

The other technique is the collinear four-point probe technique. The basic principle of the collinear four-point probe technique is to pass a current through a sample and measure the voltage drop across the sample using four probes that are arranged in a collinear configuration (Figure 4.3 (b)). The current is passed through the outer two probes, while the voltage is measured across the inner two probes. When the probes are collinear, the current flows through the sample in a straight line, which means that the voltage drop across the sample is also linear. This makes it easier to measure the voltage accurately, since any deviations from linearity can be easily detected. This technique is also designed to eliminate the effects of contact resistance, which can significantly affect the accuracy of electrical measurements. Using this technique sheet resistance (R_s) can be calculate as follows Equation (3.23):

$$R_s = \frac{\pi}{\ln 2}\frac{\Delta V}{I} \tag{3.23}$$

where ΔV is voltage measured between the inner probes, and I is the current applied between the outer probes, R_s is the sheet resistance (Mesrouk 2013). Sheet resistance refers to the electrical resistance of a thin, flat material, such as a metal film or a semiconductor wafer. It is commonly used to characterize the electrical properties of thin films and other planar structures in electronics and materials science. The relation

between resistivity, sheet resistance and film thickness (d) is as follows Equation (3.24):

$$\rho = R_s \times d \tag{3.24}$$

R_s is measured in units of ohms per square (Ω/sq) (Mesrouk 2013).

If p-type and n-type semiconductor layers are deposited on a substrate in a specific order then a p-n junction is created. As it has asymmetric current/voltage characteristics that enable the current to move in a single direction, the p-n junction operates as a rectifier diode. The current passing through the diode is given by the following Equation (3.25), depending on the voltage applied at a pn junction.

$$I = I_0 \left(e^{qV_d/nkT} - 1 \right) \tag{3.25}$$

where I_0 is called the reverse saturation current, V_d is the voltage across the diode, k is the Boltzmann constant, T is the absolute temperature, n is the ideality factor. The Equation (3.26) below expresses I_0 and it can be approximated by determining the y-intercept of the natural logarithm of I plotted against V, provided that V_d is greater than 3kT/q.

$$I_0 = AA^*T^2 exp\left(-\frac{q\Phi_b}{kT}\right) \tag{3.26}$$

where A, A^* and Φ_b represents the diode area, Richardson constant and zero barrier height, respectively (Rödl and Schleife 2014).

The diode ideality factor (η) can be found in the following manner and calculated by analyzing the slope of the lnI-V graph (Sze *et al*. 2021). The ideality factor (η) formula gives Equation (3.27).

$$\eta = \frac{q}{kT}\left(\frac{dV}{d(lnI)}\right) \tag{3.27}$$

3.2.5 Figure of merit (FoM) of a TCO

The figure of merit (also known as Quality Factor) for a transparent conductive oxide (TCO) is important because it directly affects the performance of devices that use TCOs. TCOs are widely used in various applications, including solar cells, touchscreens, flat panel displays, and light-emitting diodes (LEDs), among others. In each of these applications, the TCO must simultaneously exhibit high transparency and low electrical resistance in order to perform optimally. The figure of merit of a TCO is a measure of its overall performance, taking into account both its electrical and optical properties. The figure of merit values can be calculated using Equation (3.28).

$$\emptyset_{\mathrm{TC}} = \frac{\mathrm{T}^{10}}{\mathrm{R_S}} \tag{3.28}$$

where T is transmittance and R_s is sheet resistance. A TCO with a high figure of merit would have low sheet resistance and high optical transmittance, making it an ideal material for many applications that require transparent and conductive coatings. In addition, a TCO with a high figure of merit can help to improve the efficiency and performance of devices that use it. For example, in a solar cell, a TCO with a high figure of merit would allow more light to pass through to the active layer of the cell while minimizing energy losses due to resistive losses (Haacke 1976).

4. RESULTS AND DISCUSSIONS

In this section, the production and characterization results of NiO films deposited on different substrates (Glass-FTO-ITO) with the SILAR technique are given. Structural, optical, surface and electrical characterizations of NiO-Glass, NiO-FTO and NiO-ITO films were made and the results were explained.

4.1. Production of NiO/FTO-NiO/ITO-NiO/GLASS

In this study, the production and characterization of NiO films on different substrates were carried out using the sequential ion layer adsorption and reaction (SILAR) method. The effect of the substrates used in the SILAR technique used in the production of NiO films was investigated. In addition, the changes made by the substrate used on the physical and chemical properties of NiO films were determined.

4.1.1 Substrate preparation

Glass, FTO, ITO, and glass materials were used as the substrate for the growth of the films. The glass substrates were cut to 8 mm wide and 25 mm long. After the cutting process, the glass substrates, FTO, ITO, and glass were washed thoroughly with soapy water to get rid of dirt. After washing, the substrates were ultrasonically cleaned in acetone for 10 minutes. The clean FTO, ITO, and glass substrates were then dried in nitrogen gas. All prosesses were performed at room temperature.

4.1.2 Solutions preparation

Solutions were prepared to obtain nickel oxide layers by dissolving nickel (II) nitrate and aqueous ammonia in distilled water in a flask (one hundred milliliters) to obtain a ketone precursor and form compound ions) $[Ni(NH_3)_4]^{+2}$ with (pH≈10), where the reagents are used analytically for $NiCl_2$ and concentrated ammonia (NH_3) (28 %). The specific concentration values for a nickel (Ni) solution were 0.1 M and the molar ratio

of Ni:NH_3 was 1:10 obtained as a result of several experiments. The SILAR growth cycle consists of four successive steps:

(i) Dipping the substrate into the $[Ni(NH_3)_4]^{+2}$ complex solution for 30 seconds to create a thin liquid film containing $[Ni(NH_3)_4]^{+2}$ on the substrate; (ii) immediately dipping of the extruded substrates into hot water (90 °C) for 7 seconds to form a NiO layer; (iii) dry the substrates in the air for 60 sec and (iv) then keep them in distilled water at room temperature for 30 minutes. Thus, the SILAR cycle is completed. The diagram showing the precipitation steps with the SILAR method to obtain nickel oxide films is shown in Figure 4.1.

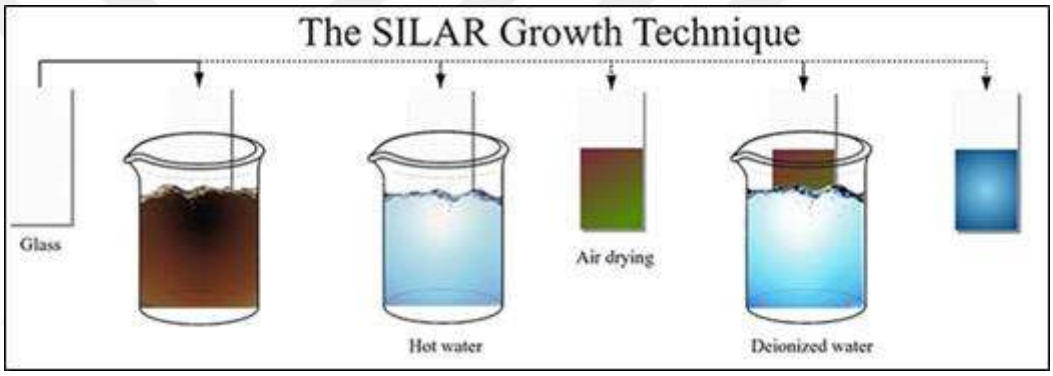

Figure 4.1 Diagram representing the steps of sedimentation by the SILAR method to obtain nickel oxide films

The mass of nickel (II) nitrate to be added is determined by the following relationship Equation (4.1):

$$m = C \times M \times V \quad (4.1)$$

where *C* is the molar concentration (mol/L), *V* is solution volume (L), *M* is the molar concentration of nickel (II) nitrate = 290.79 g/mol, *m* (mg) is the mass of nickel (II) nitrate and be added to the solution. The process was repeated 40 times for all samples under the same conditions and annealing temperature for 15 minutes in an annealing

furnace (Figure 4.2). The thickness of the produced films was determined by the weight method and calculated as approximately 200 nm for NiO-Glass, NiO-FTO and NiO-ITO films.

Figure 4.2 Annealing Furnace

4.2 Characterization of NiO Films

The structural, optical, electrical and surface properties of NiO-ITO, NiO-FTO, NiO-Glass films deposited on different substrates were investigated. X-ray diffactometer (XRD), UV-VIS spectrophotmeter, current-voltage measurment system (I-V) and field emission scanning electron micrsocopy (FESEM) were used in the characterization of the specified properties.

The UV-VIS spectrometer was used for optical analysis in Figure 4.3. Absorbance and transmittance spectra were obtained from UV-vis spectrometer analyses. By using these spectra, band gap, band structure, Urbach energies, refractive indes values and transmittance of NiO films were determined. An APD 2000 PRO XRD device was

used to analyze the X-ray results (Figure 4.4). X-ray diffraction patterns of NiO films were obtained from XRD analysis. Using these patterns, crystallization levels, grain sizes, lattice constants, half-peak widths and dislocation densities of NiO films were calculated.

The electrical properties of the films were determined by the two-end method. By making contact at two different points on the films, voltages in the range of -3 and +3 volts were applied, and the current values of current against these voltages were determined. I-V graphs were drawn from the obtained current (I)-voltage (V) values and the transmission mechanisms were determined.

In addition, electrical parameters such as barrier height and ideality factor of NiO films were also calculated. The scaning elecrton microscopy (FESEM) characterization technique for morphological properties and the effect of the base used on the surface properties of the films was investigated. The surface images of the films were obtained in general and the effect of the substarte used on the surface properties was examined.

Figure 4.3 UV-VIS spectrometer

Figure 4.4 APD 2000 PRO XRD device

4.2.1 Structural characterization of NiO/FTO-NiO/ITO-NiO/GLASS

All XRD patterns of NiO-ITO, NiO-FTO, NiO-Glass films are given in Figures 4.5, 4.6, 4.7 and 4.8. When Figure 4.5 is examined, it has been determined that the material with the best crystallization level of NiO films is NiO-ITO. NiO-Glass films have the lowest crystallization level compared to other films. While the crystallization level of NiO-FTO films is worse than NiO-ITO films, it is better than that of NiO-Glass films. The 'd' values observed according to the XRD results of the NiO films are in good agreement with the standard 'd' values. All films were determined to form in the cubic phase of NiO acoording to the Joint Committee on Powder Diffraction Standards card (JCPDS:01-073-1519) and the diffraction peaks were indexed. The diffraction peaks were found as a=b=c=4.165° for NiO-Glass films, a=b=c=4.157° for NiO-ITO films and a=b=c=4.154° for NiO-FTO films. In addition, it was determined that the dominant growth in all films was in the (111), (200), (220) directions. Also, the structural parameters such as lattice conctants (a, b and c), grain size (D), dislocation density (d), FWHM and microstress (ε) for all films calculated and these results are given for NiO-GLASS, NiO-FTO and NiO-ITO filmsin Tables 4.1, 4.2 and 4.3, respectivily.

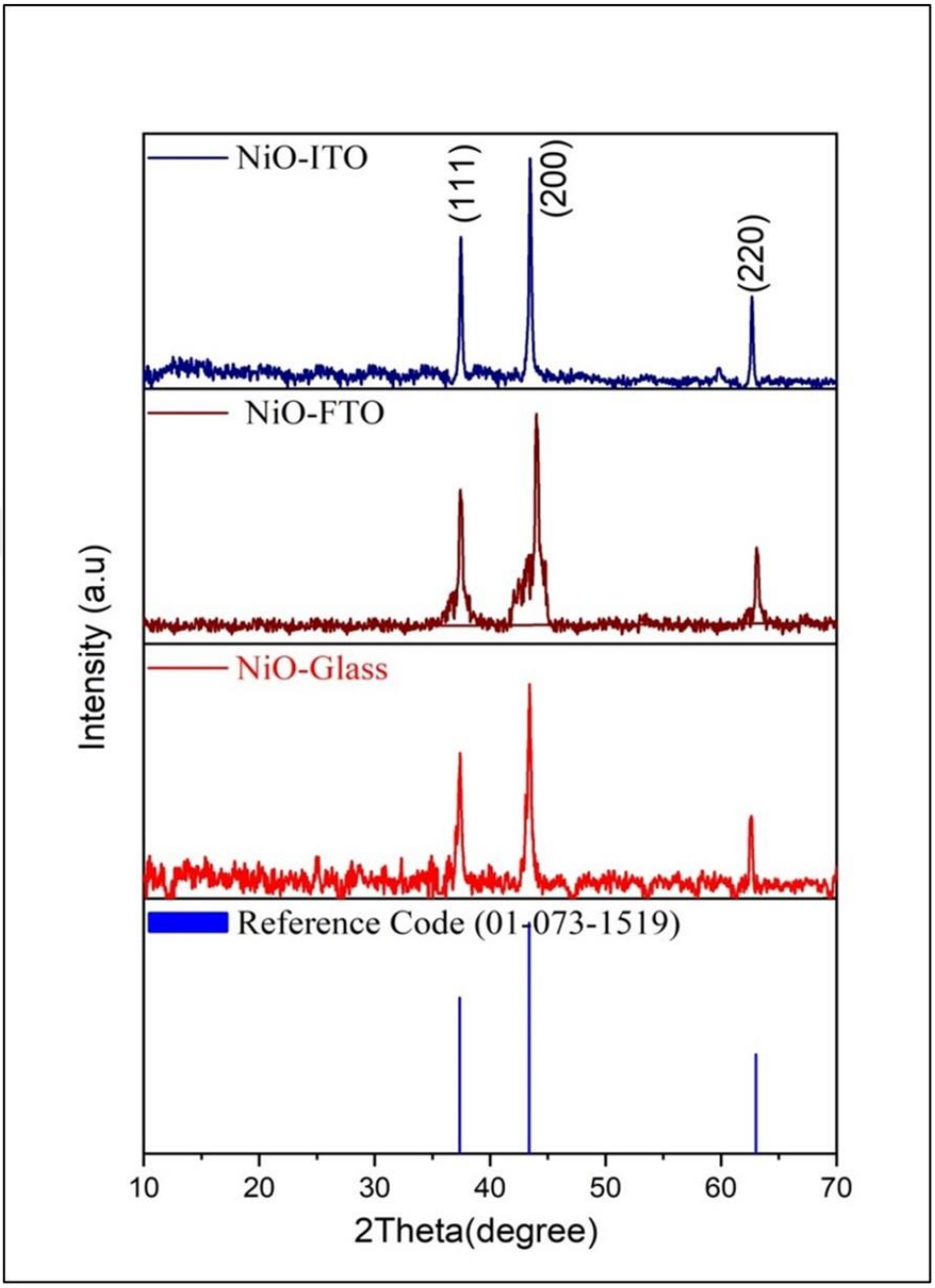

Figure 0.5 X-ray analysis of (NiO-ITO, NiO-FTO, NiO-Glass) films

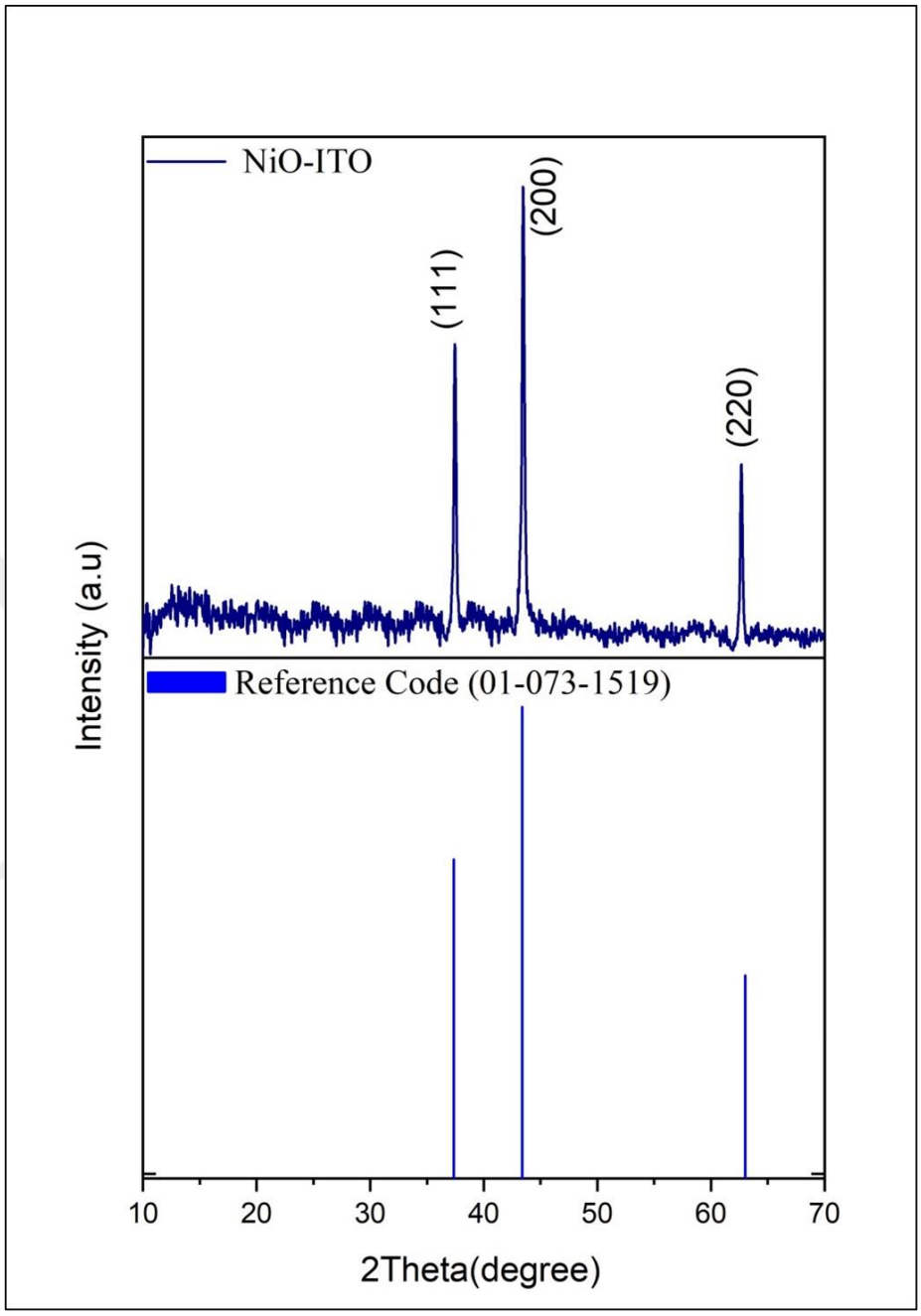

Figure 0.6 X-ray analysis of (NiO-ITO) film

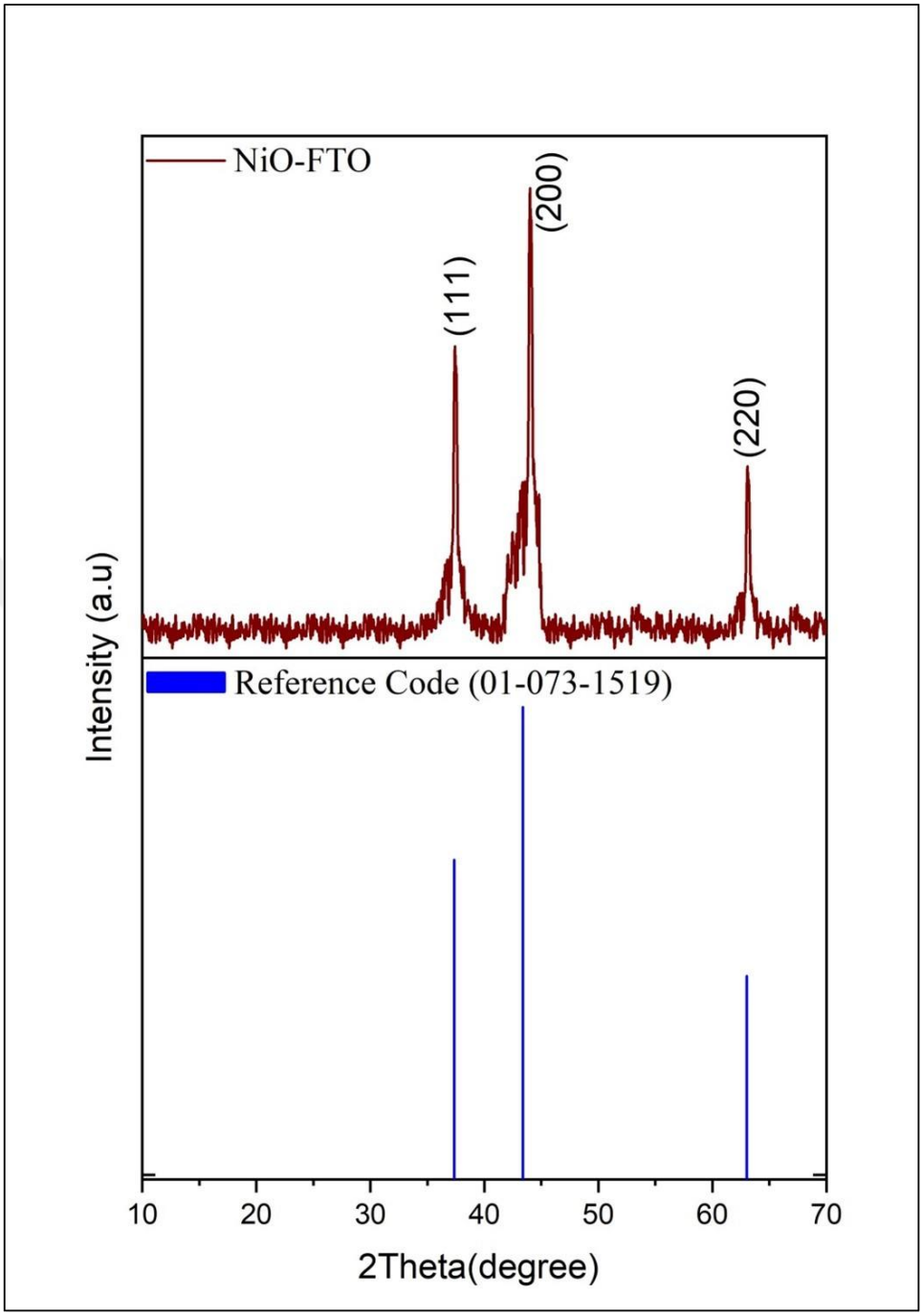

Figure 0.7 X-ray analysis of (NiO-FTO) film

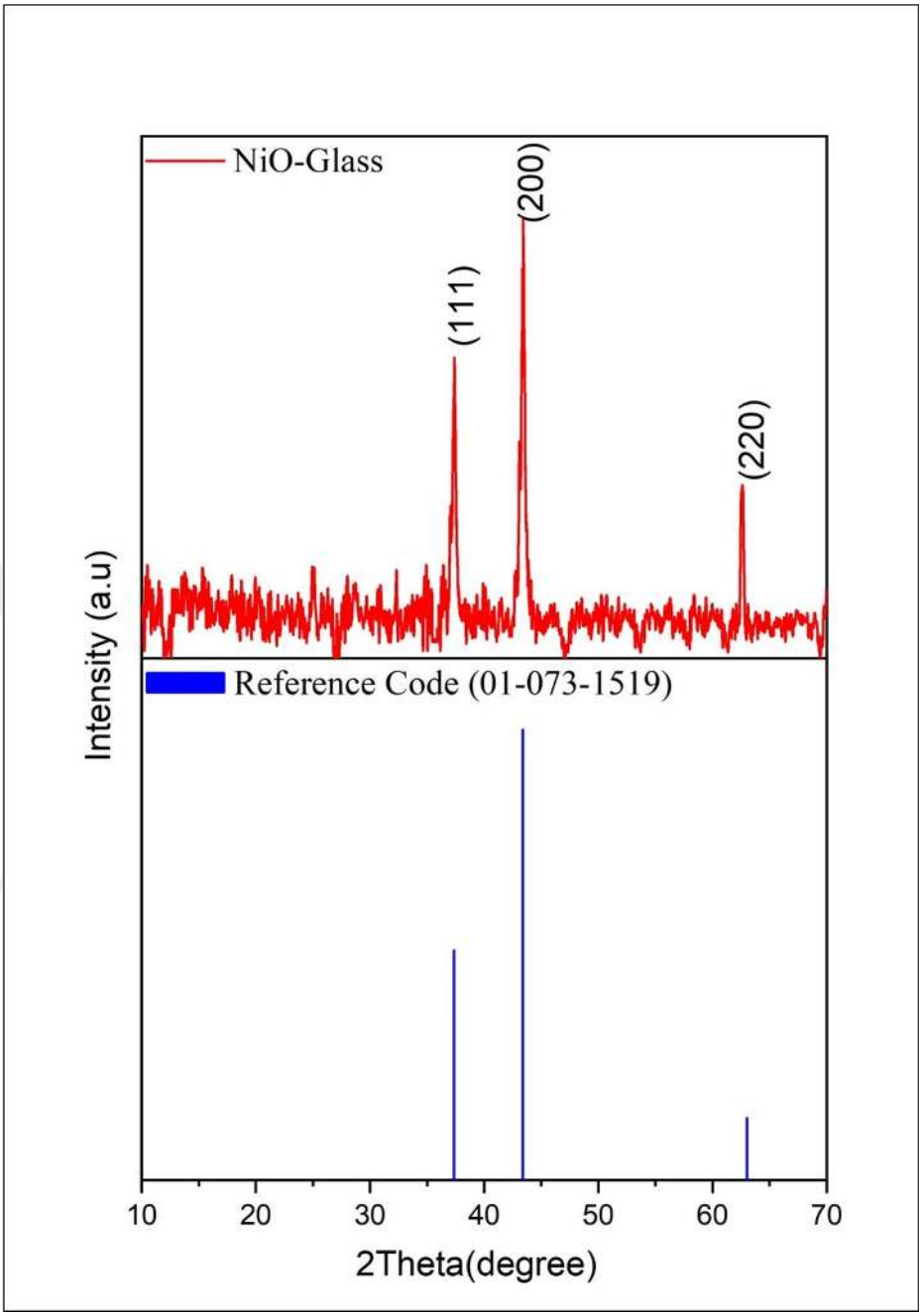

Figure 0.1 X-ray analysis of (NiO-Glass) film

Table 0.1 Some structural parameters of NiO-Glass

Angle (2θ°)	FWHM (°)	d-SPACE STANDARD (Å)	GRAIN SIZE (nm)	ε ($Lines^{-2}nm^{-4}$)	δ ($Lines/nm^2$)	LATTICE PARAMETER (Å) a =b=c
37.35	0.16294	0.240459	51.44593	0.6735×10^{-4}	3.77×10^{-4}	4.165
43.39	0.2908	0.208251	29.39095	1.178×10^{-4}	11.57×10^{-4}	
62.59	0.15556	0.148231	59.74177	0.579×10^{-4}	2.80×10^{-4}	

Table 0.2 Some structural parameters of NiO-FTO

ANGLE (2θ°)	FWHM (°)	d-SPACE STANDARD (Å)	GRAIN SIZE (nm)	ε ($Lines^{-2}nm^{-4}$)	δ ($Lines/nm^2$)	LATTICE PARAMETER (Å) a =b=c
37.45	0.174	0.239	48.162	0.719×10^{-3}	4.311×10^{-4}	4.154
43.66	0.260	0.207	32.857	1.051×10^{-3}	9.262×10^{-4}	
63.06	0.161	0.147	57.636	0.598×10^{-3}	3.01×10^{-4}	

Table 0.3 Some structural parameters of NiO-ITO

ANGLE (2θ°)	FWHM (°)	d-SPACE STANDARD (Å)	GRAIN SIZE (nm)	ε ($Lines^{-2}nm^{-4}$)	δ ($Lines/nm^2$)	LATTICE PARAMETER S(Å) a =b=c
37.45	0.250	0.239	33.444	1.033×10^{-3}	8.940×10^{-4}	4.157
43.48	0.290	0.207	29.421	1.175×10^{-3}	1.155×10^{-4}	
62.71	0.254	0.147	36.591	0.946×10^{-3}	1×10^{-4}	

4.2.2 Morphological characterization of NiO/FTO-NiO/ITO-NiO/GLASS

A Field Emission Scanning Electron Microscope (FESEM) was used to examine the surface morphology of the films NiO-Glass, NiO-FTO, NiO-ITO deposited on substrates. Figure 4.9 shows FESEM images of deposited films. It is clear that the surfaces of the prepared films have round particles, with a homogeneous distribution on the substrate, and there are no cracks on the surface of the film or large molecular agglomerations. The formation of the film surface depends on the method of preparation and deposition parameters of the SILAR method. The surface homogeneity of the films deposited on the FTO and ITO substrates was determined well than the surface homogeneity of the NiO films deposited on the glass substrate. While cracks occur in some places on the surfaces of the films deposited on the glass, other films are completely homogeneous. The most homogeneous NiO films are those deposited on ITO. In all films, Ni and O atoms combined to form a round structure. In NiO films produced on ITO base, these round formations are more prominent and larger than other films.

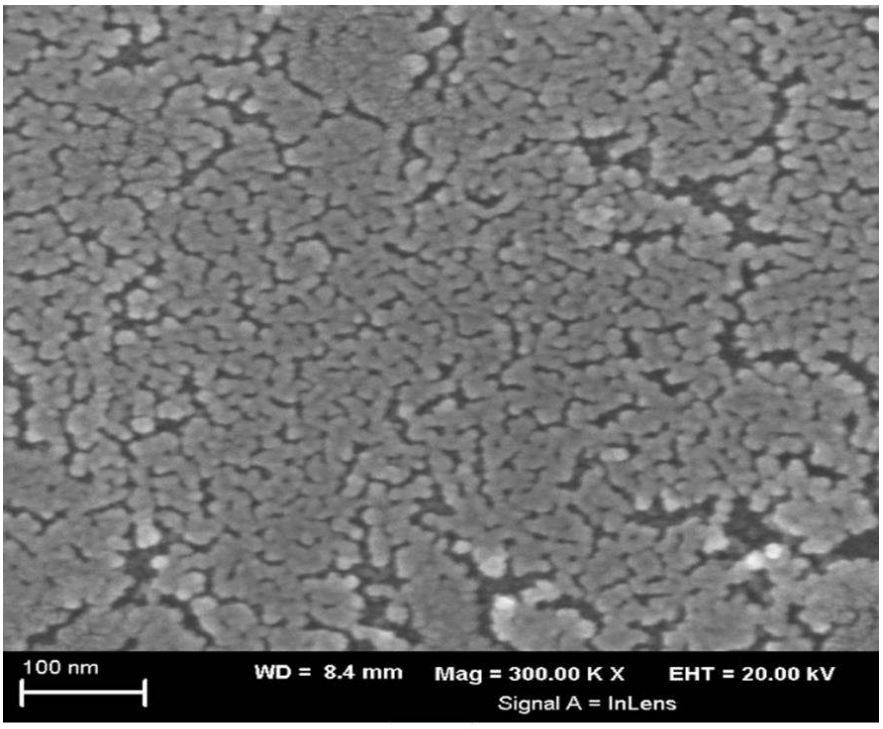

(a)

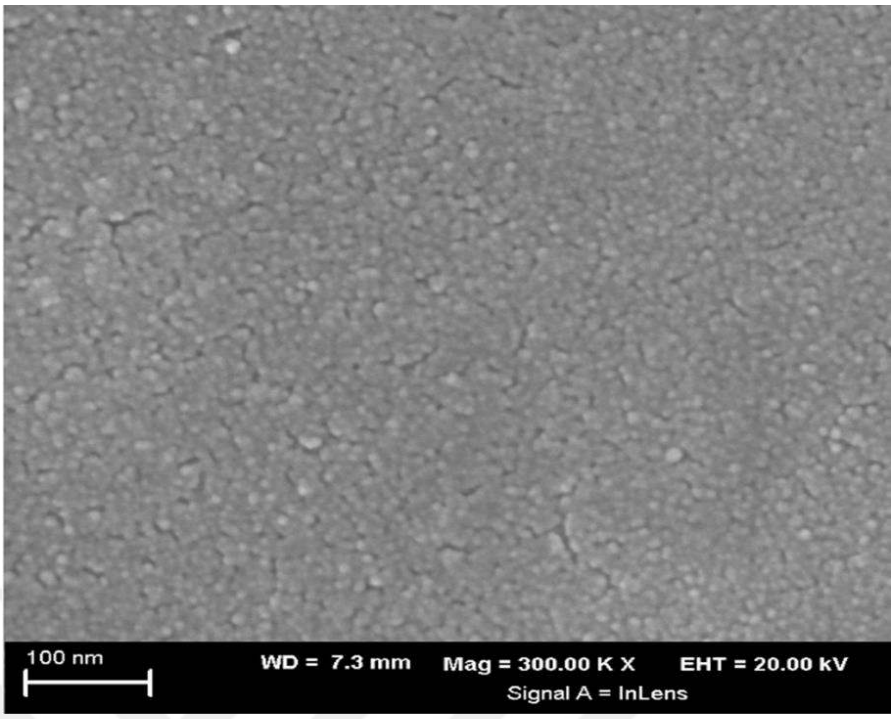

(b)

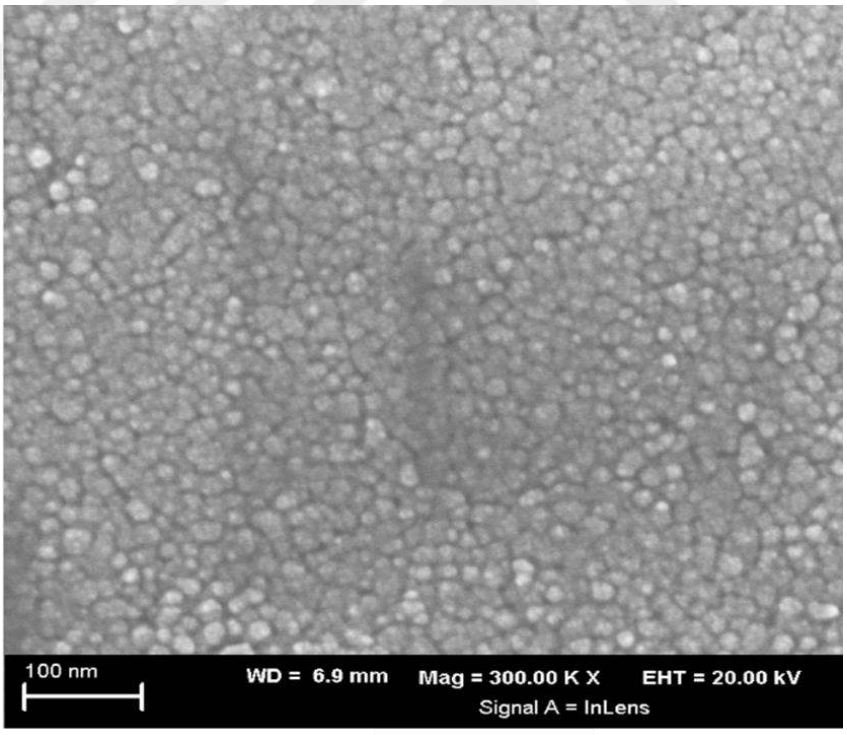

(c)

Figure 4.9 FESEM images of (a) NiO-Glass, (b) NiO-FTO and (c) NiO-ITO films

4.2.3 Optical characterization of NiO/FTO-NiO/ITO-NiO/GLASS

By using the absorption and transmittance spectra of NiO films obtained from UV-VIS spectrometry, some optical parameters such as band structure, band gap (E_g), Urbach energy (E_u), refractive index (n).

The optical properties of materials are essential in many industrial and laboratory fields for several reasons, including using these materials in optical fibers (and reflective coatings) which require accurate knowledge of their optical constants over a wide range of wavelengths, as well as. The correlation of the optical properties of all materials with their atomic structure and the importance of studying the optical properties of transparent conductive oxides lies in their wide use of them in many industrial and laboratory fields. These characteristics are the following: transmittance (T), reflectance (R), absorption (A) and absorption coefficient α, and other properties (Heavens 1991) and these graphics are given in Figures 4.10, 4.11, and 4.12 for NiO films, respectively.

Depending on UV-VIS results, some optical properties of pure nickel oxide deposited using a SILAR method on glass substrates (NiO-ITO, NiO-FTO, NiO-Glass) were calculated, which can be summarized in Table 4.4. Figure 4.10 shows the transmittance spectrum of NiO films (NiO-ITO, NiO-FTO, NiO-Glass) produced on different substrates by the (SILAR) method. It was determined that the material with the highest average permeability value in the visible region was NiO-ITO, while the lowest material was NiO-Glass. It has been seen that ITO bases are more suitable than others to obtain high transmittance values in NiO films. Absorption spectra of NiO films are given in Figure 4.11. When the absorption spectra are examined, it is seen that the band edge of the NiO-Glass films has a more flat and distorted structure. This situation is slightly improved for NiO-FTO and these films have smoother band edges than NiO-Glass films. On the other hand, it was determined that the band edge of NiO-ITO films became sharper and the band structure improved. In addition, a graph showing the change of refractive index values of NiO films according to wavelength is

drawn and given in Figure 4.12. It was determined that the average refractive index values of the films in the visible region ranged between 1.5 and 2.

Table 0.4 Some results of optical properties of the films

MATERIALS	NiO-ITO	NiO-FTO	NiO-Glass
λ (nm)	350-900	350-950	350-900
Transmittance (T)	30-50 %	17- 47 %	15-40 %
Absorption (A)	53-28 %	77 -33 %	83-40 %
Reflectivity (R)	17-22 %	6-20 %	2-20 %

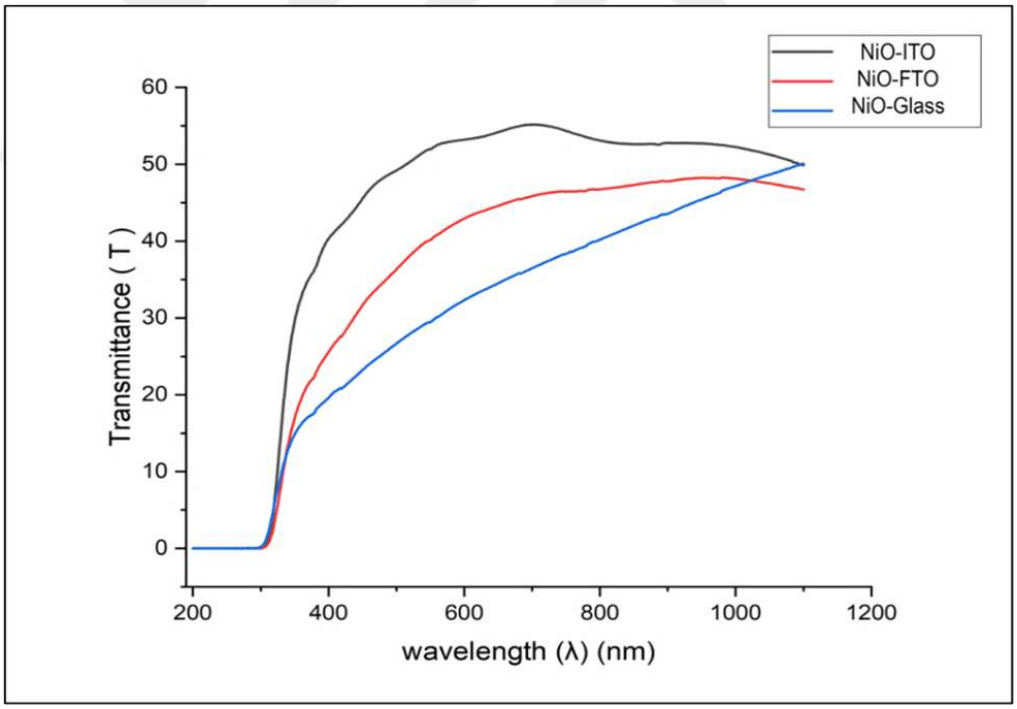

Figure 0.2 Transmittance of (NiO-ITO, NiO-FTO, NiO-Glass) as a function of wavelength

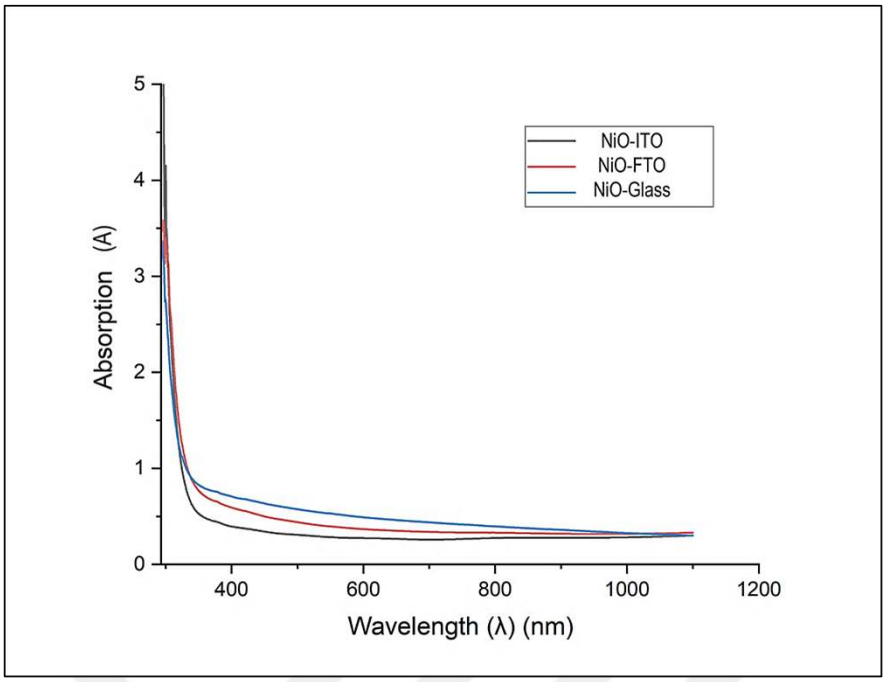

Figure 0.3 Absorbance of (NiO-ITO, NiO-FTO, NiO-Glass) as a function of wavelength

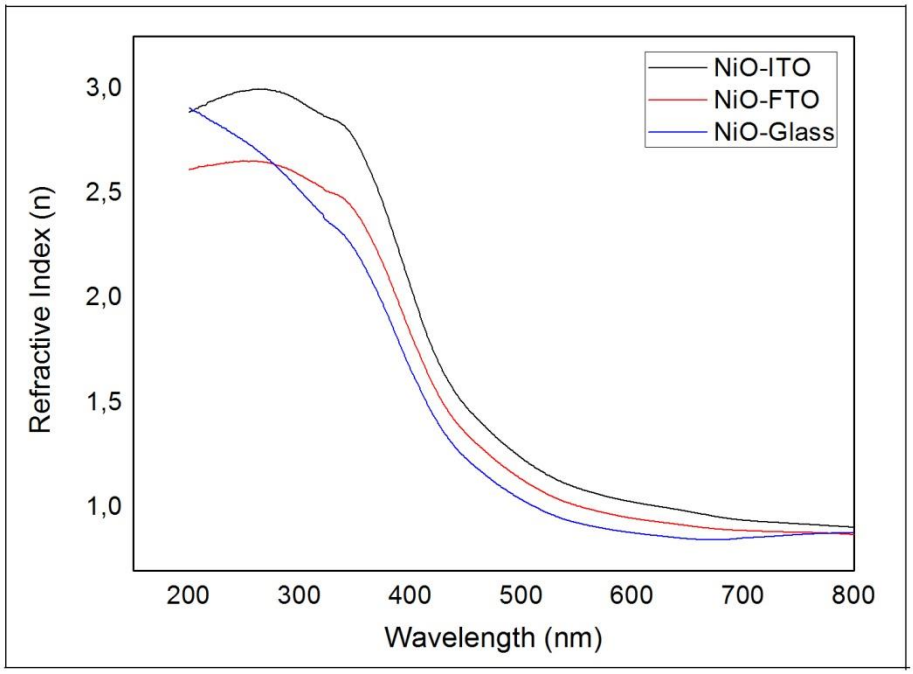

Figure 0.4 Refractive index of films (NiO-ITO, NiO-FTO, NiO-Glass) as a function of wavelength

Band gap values were calculated by optical method by using the absorbance spectra of NiO-ITO, NiO-FTO, NiO-Glass films deposited on different substrates by SILAR method. Graphs 4.13 to 4.18 show the optical energy gap of NiO films for direct and indirect electron transitions. While the calculated indirect optical energy gap value was in the range (3.56 – 3.68 eV), the direct optical energy gap values were determined to be in the range of 3.92-3.97 eV. The calculated band gap energy values of Nickel oxide films produced on ITO, FTO and Glass are 3.91, 3.93 and 3.97 eV, respectively. Band gap values of NiO films produced on ITO and FTO substrates are almost the same. However, band gap values of NiO films produced on glass are higher than films produced on other substrates. NiO films produced on glass substrates have the widest band gap (3.97 eV) for direct band transition. were determined.

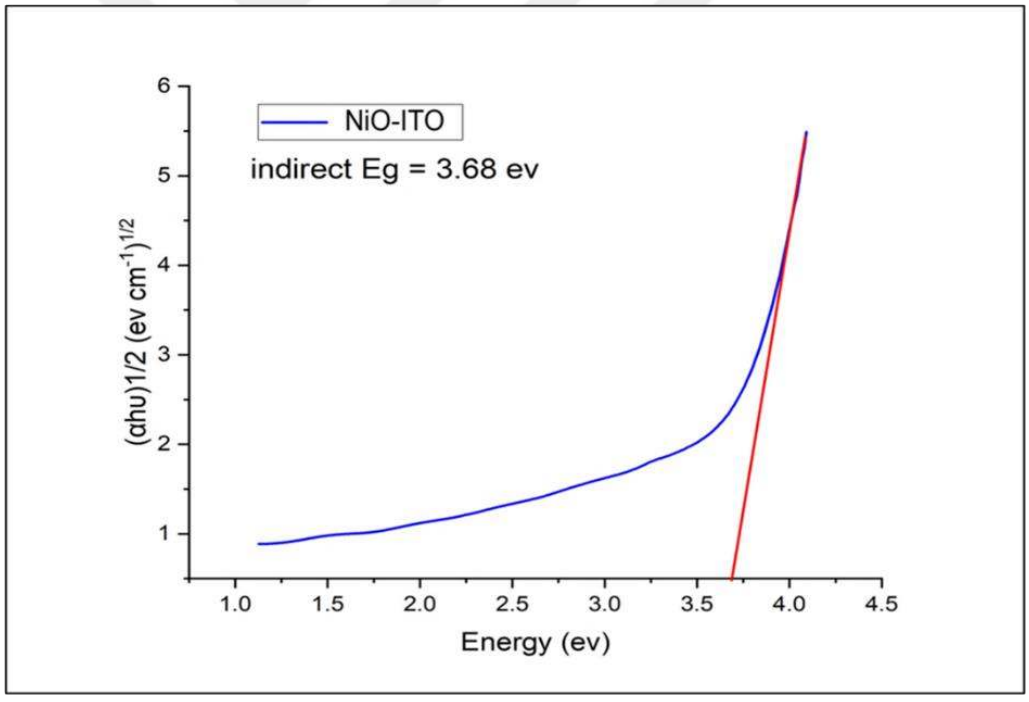

Figure 0.53 Indirect Energy gap of (NiO-ITO) films

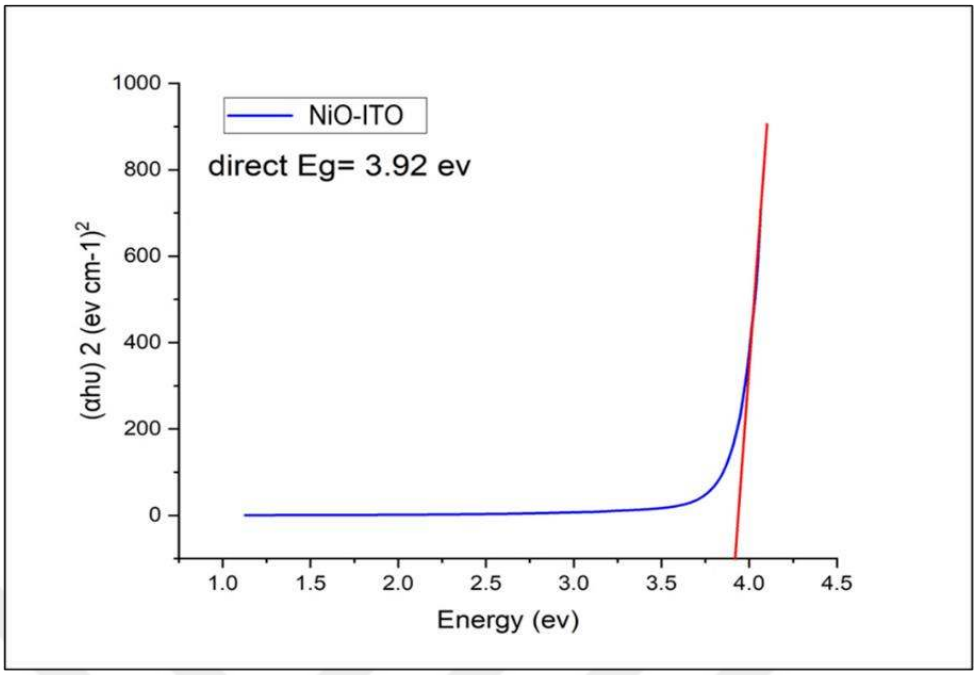

Figure 0.14 Direct Energy gap of (NiO-ITO) films

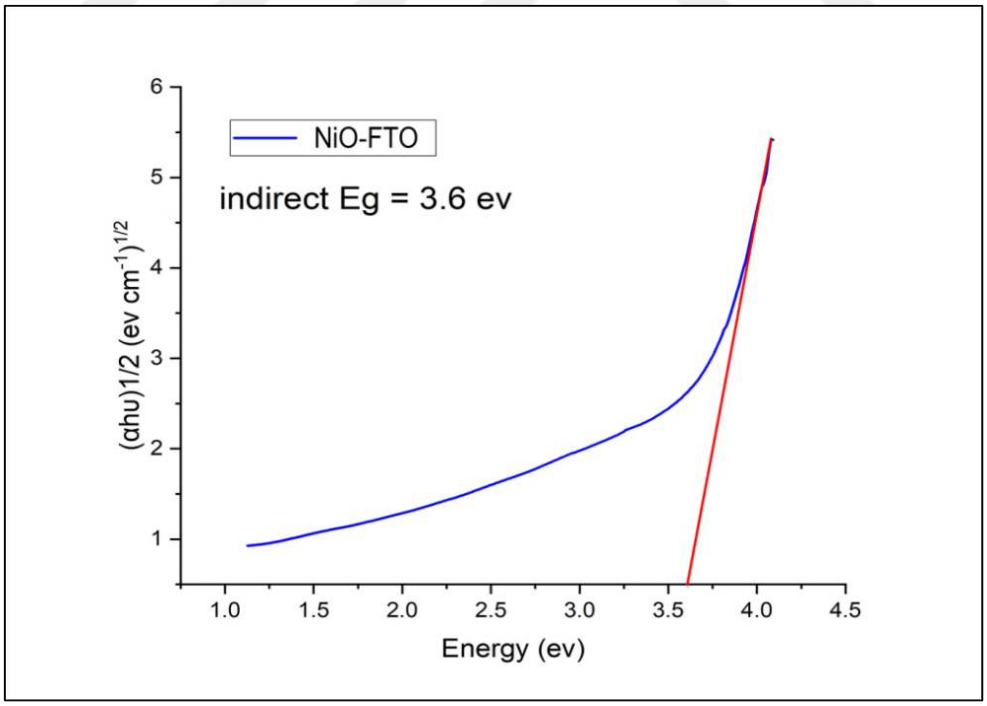

Figure 0.15 Indirect Energy gap of (NiO-FTO) films

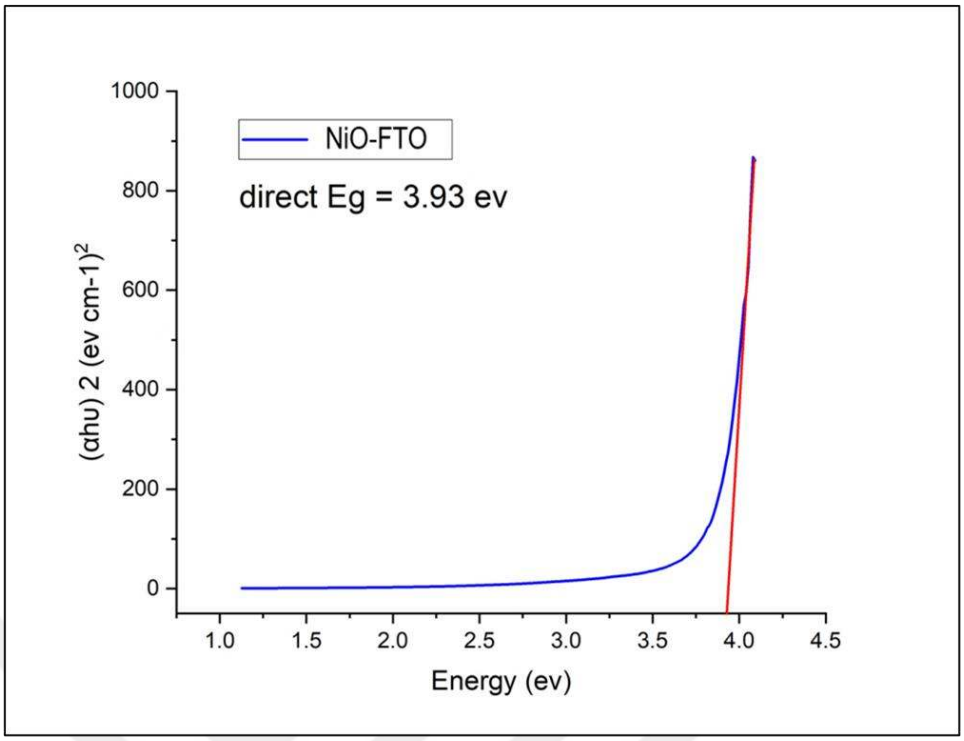

Figure 0.16 Direct Energy gap of (NiO-FTO) films

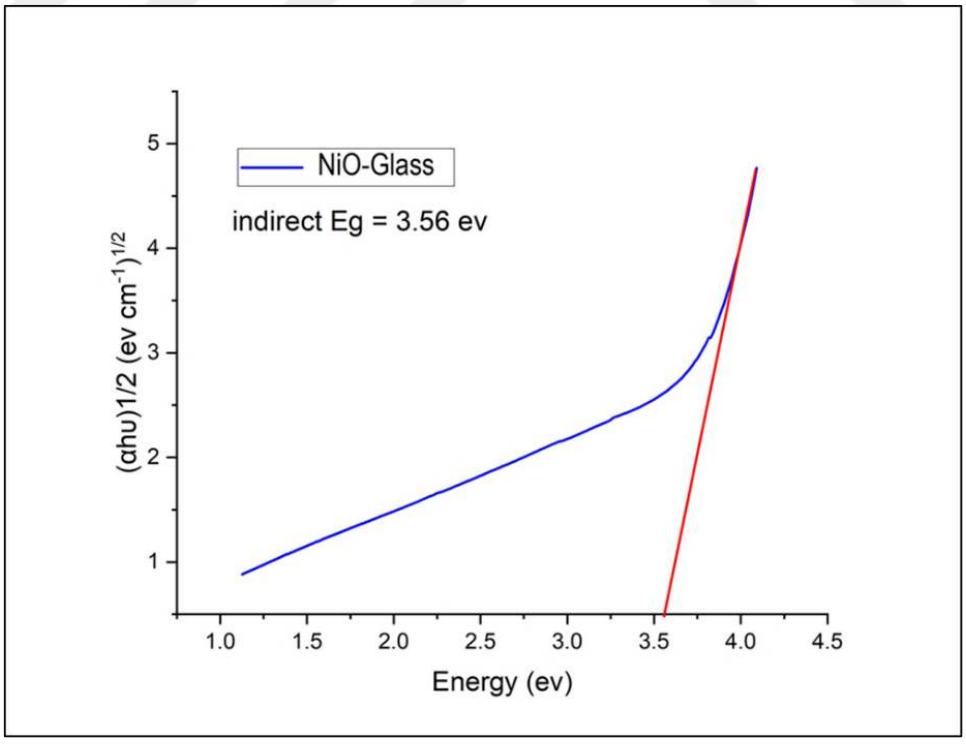

Figure 0.17 Indirect Energy gap of (NiO-Glass) films

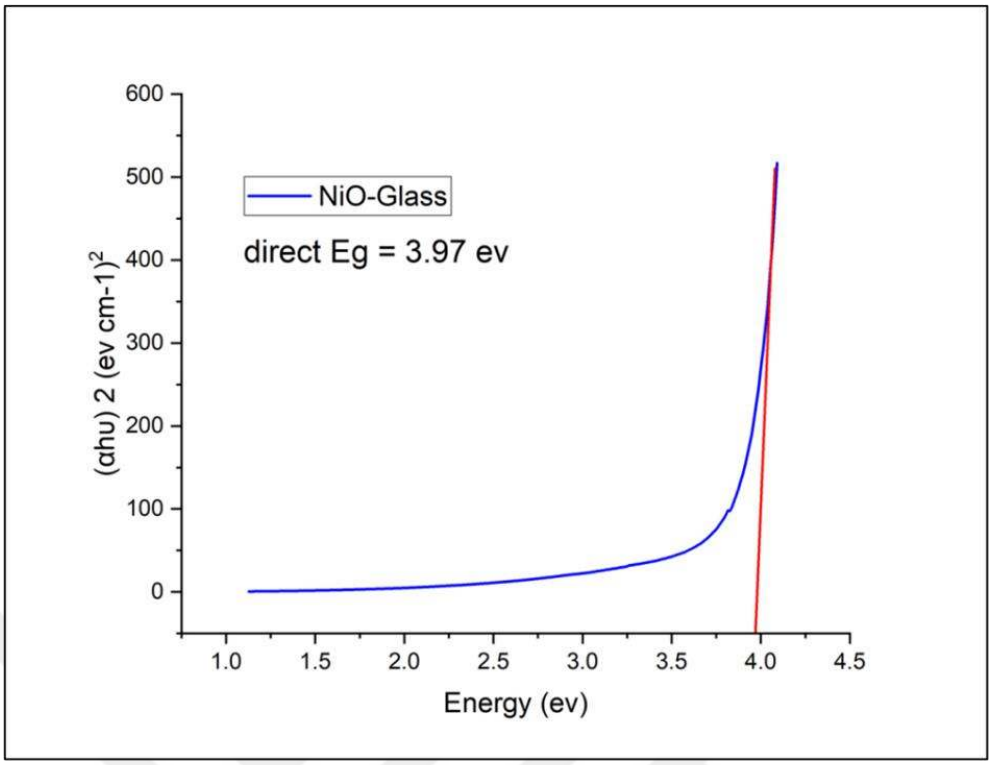

Figure 0.18 Direct Energy gap of (NiO-Glass) films

The Urbach energy is one of the important constants that characterize the optical properties of the thin layer. It expresses the relationship between the Urbach energy and the absorption coefficient. depends on the energy of the photon in the spectral range of the edge of the near band, which is an empirical exponential law (Urbach's tail) (Gençyılmaz 2021).

The graphs in Figures 4.19 to 4.21 show plotting the curve of the change in photon energy ($h\nu$) in terms of ($Ln\alpha$). Calculation Urbach Energy for pure NiO films deposited on glass substrates (NiO-ITO, NiO-FTO, NiO-Glass) was calculated based on the above and using UV-VIS calculations. The calculated Urbach energy values of NiO films produced on ITO, FTO and Glass are 0.26, 0.31 and 0.36 eV, respectively. In nickel oxide films, the highest Urbach energy was in the production on glass, and the lowest Urbach energy was in the production on ITO base. This indicates that the material with the least energetic irregularity at the band edges in terms of the substrates used is NiO-ITO.

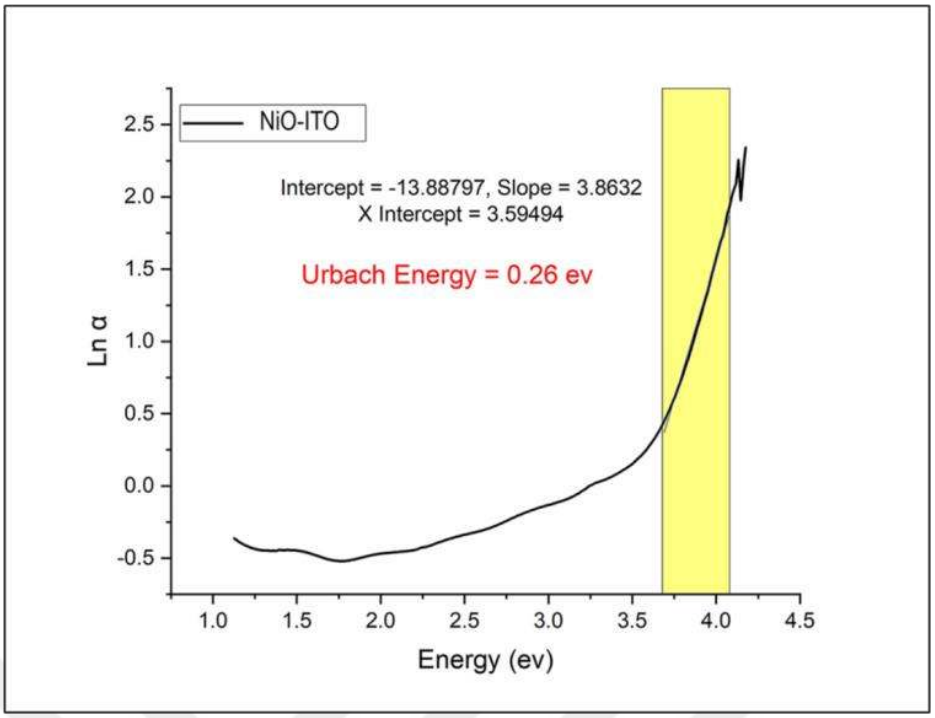

Figure 0.19 Urbach Energy (NiO-ITO) film

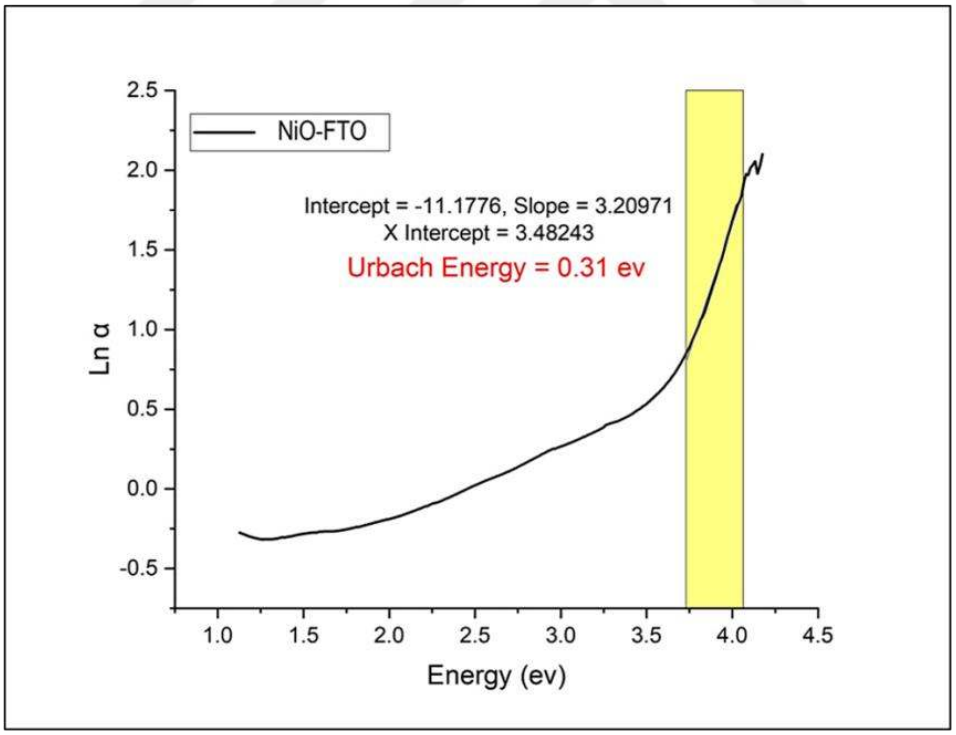

Figure 0.20 Urbach energy of (NiO-FTO) film

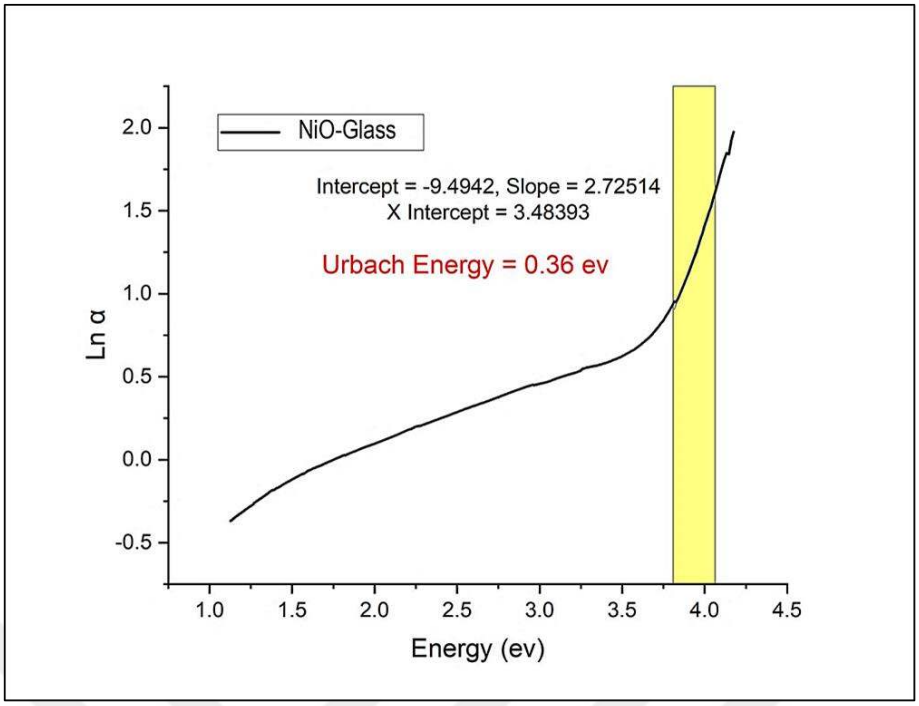

Figure 0.21 Urbach energy of (NiO-Glass) film

4.2.4 Electrical characterization of NiO/FTO-NiO/ITO-NiO/GLASS

The two-point method was used to examine the sheet resistance (R_s). A variation in the voltage (V) was applied between the outer two leads and the current (I) was measured under dark conditions. The reverse to forward bias current measurement was taken for the applied potential of –3 V to +3 V. This method was applied linearly and the layer resistance was calculated.

Figure 4.22, Figure 4.23 and Figure 4.24 shows the I-V characteristics of NiO films under dark. Through the graph and the values of the surface resistance, the results showed that Nickel oxide films deposited on glass substrates (NiO-Glass) exhibit linear ohmic behavior in both cases of forward and reverse bias as shown in Figure 4.22. The films deposited on glass Fluorine-doped tin oxide (NiO-FTO) showed a nonlinear behavior closer to exponential than ohmic behavior in both forward and reverse bias cases as shown in Figure 4.23.

Based on the obtained I-V results, the surface resistance and electrical conductivity values of the films shows by two Tables 4.5 and 4.6 following. It is seen that the conductivity of NiO-ITO and NiO-FTO films is higher than NiO-Glass in the forward and reversse bias of conductivity. This observation of increase in conductivity can be explained by the tail width of localized states within the optical bandgap (Urbach energy), depending on the nature of the substrate used. In addition, changes in the crystal structure of the films may cause an improvement in electrical conductivity.

Table 0.5 The surface resistance values in the forward bias

MATERIAL	**V (VOLT)**	**R_S (Ω)**	**σ (Ω.cm)**
NiO-ITO	3-0.05	7.32×10^{2}	6.83×10^{1}
NiO-FTO	3-0.05	2.88×10^{3}	1.73×10^{1}
NiO-Glass	3-0.05	9.26×10^{3}	5.40

Table 0.6 The surface resistance values in reverse bias

MATERIAL	**V (VOLT)**	**R_S (Ω)**	**σ (Ω.cm)**
NiO-ITO	(-3) - (-0.05)	2.68×10^{3}	1.87×10^{1}
NiO-FTO	(-3) - (-0.05)	6.17×10^{3}	8.10
NiO-Glass	(-3) - (-0.05)	9.77×10^{3}	5.12

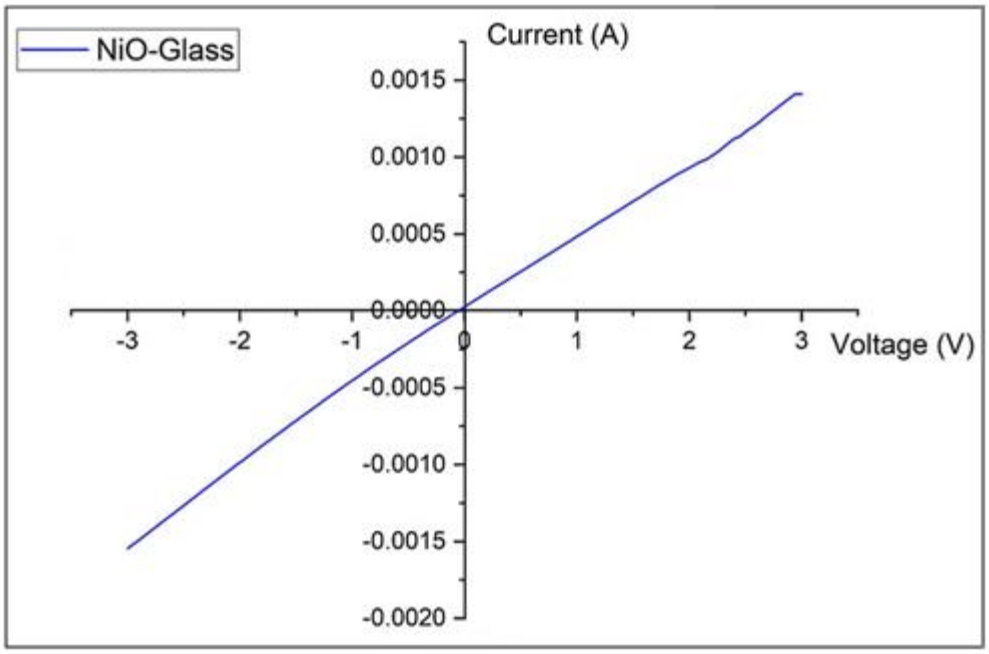

Figure 0.22 Voltage and current curve of (NiO-Glass) film

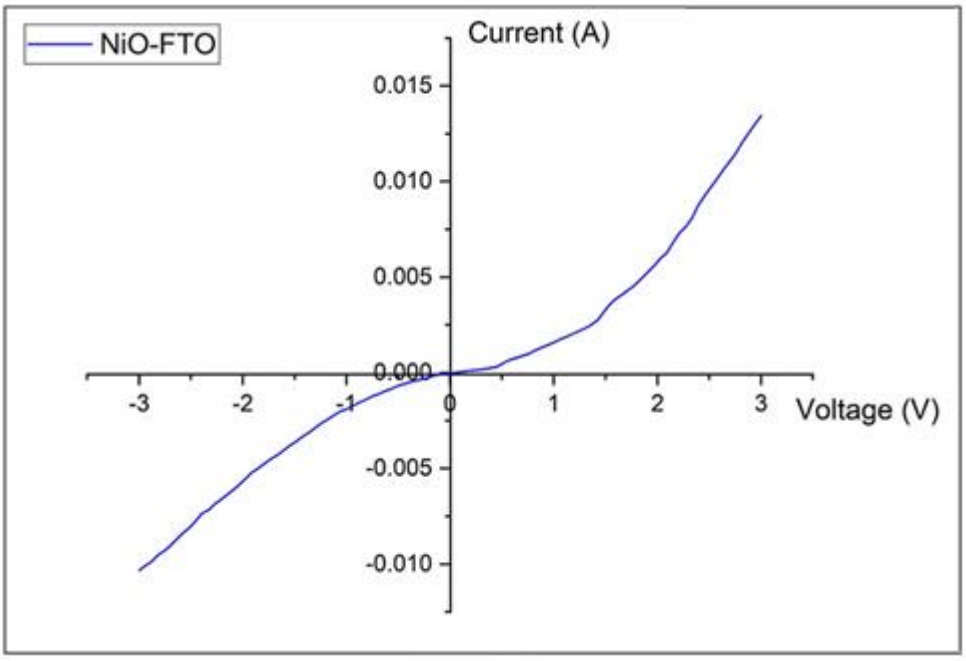

Figure 0.23 Voltage and current curve of (NiO-FTO) film

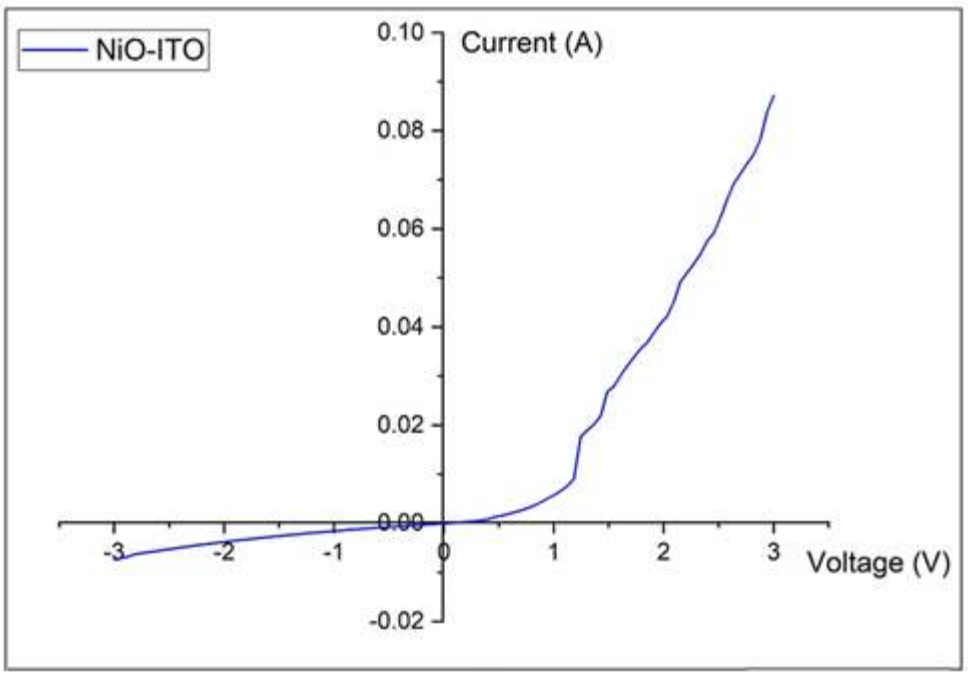

Figure 0.6 Voltage and current curve of (NiO-ITO) film

To determine the charge transport mechanism of the NiO films, a conventional current Equation (4.16) is used as;

$$I = I_0 \left[exp \frac{qV}{nkT} \right] \tag{4.16}$$

where V is the applied voltage, n is the ideality factor, k is the Boltzmann constant, T is the absolute temperature and q is the electronic charge, I_0 is the saturation current,. I_0 is the saturation current given by Equation (4.17);

$$I_0 = AA^*T^2 exp\left(-\frac{q\phi_B}{kT}\right) \tag{4.17}$$

where b, A, A^*, are the zero-bias barrier height, effective contact area and effective Richardson's constant respectively. The theoretical value of Richardson's constant is expressed as in Equation (4.18).

$$A^* = \frac{4\pi m^* K^2 q}{h^3} \tag{4.18}$$

where h is the Planck's constant and m^* is the effective mass of electron. Here we put $m^* = 0.8m_0$ for NiO to get the value of effective Richardson's constant, and the calculated value was found to be $A^* \sim 96$ A-cm^{-2}-K^{-2} (Rödl and Schleife 2014).

The prepared NiO films parameters barrier height Φ_B and ideality factor η were measured under dark conditions. The reverse to forward bias current measurement was taken for the applied potential of –3 V to +3 V. By using the theory of thermoionic emission and using I-V results of the deposited films, the parameters barrier height ϕ_B, ideality factor η were measured by the following Equations (4.19) and (4.20).

$$\phi_B = \frac{K_b T}{q} \mathrm{Ln}\left(\frac{AA^* T^2}{I_0}\right) \tag{4.19}$$

where ϕ_B is barrier height at zero bias and by putting all the values in Equation (4.17) and (4.28) the barrier height ϕ_B was calculated.

The ideality factor (η) which is another important electrical parameter were calculated by the following Equations (4.20);

$$\eta = \frac{q}{K_b T}\left(\frac{dV}{d(\mathrm{Ln}I)}\right) \tag{4.20}$$

The log I-V plots of NiO films is given in Figure 4.20, Figure 4.21 and Figure 4.22. Could $\left(\frac{dV}{d(\mathrm{Ln}I)}\right)$ obtained from the I-V graph in Figure 4.20, Figure 4.21 and Figure 4.22. And we got the η valuses (Sze *et al*. 2021). Table 4.10 shows some electrical parameters calculated. These results are roughly consistent with previous studies (Stamataki *et al*. 2008, Castro *et al*. 2013, Saju and Balasundaram 2019).

The films (NiO-ITO) and (NiO-FTO) showed slightly different electrical behvior than the other samples, as this sample has characteristics close to a diode and a small saturation current compared to the other samples as shown in the Figure 4.25 and 4.26.

The electrical properties of NiO films show that these films are suitable for photodetector applications.

Table 0.7 The some electrical parameters calculated

FİLMS	**η**	**ϕ_B (eV)**
NiO-ITO	1.4420	0.554
NiO-FTO	1.9756	0.494
NiO-GLASS	3.4480	0.589

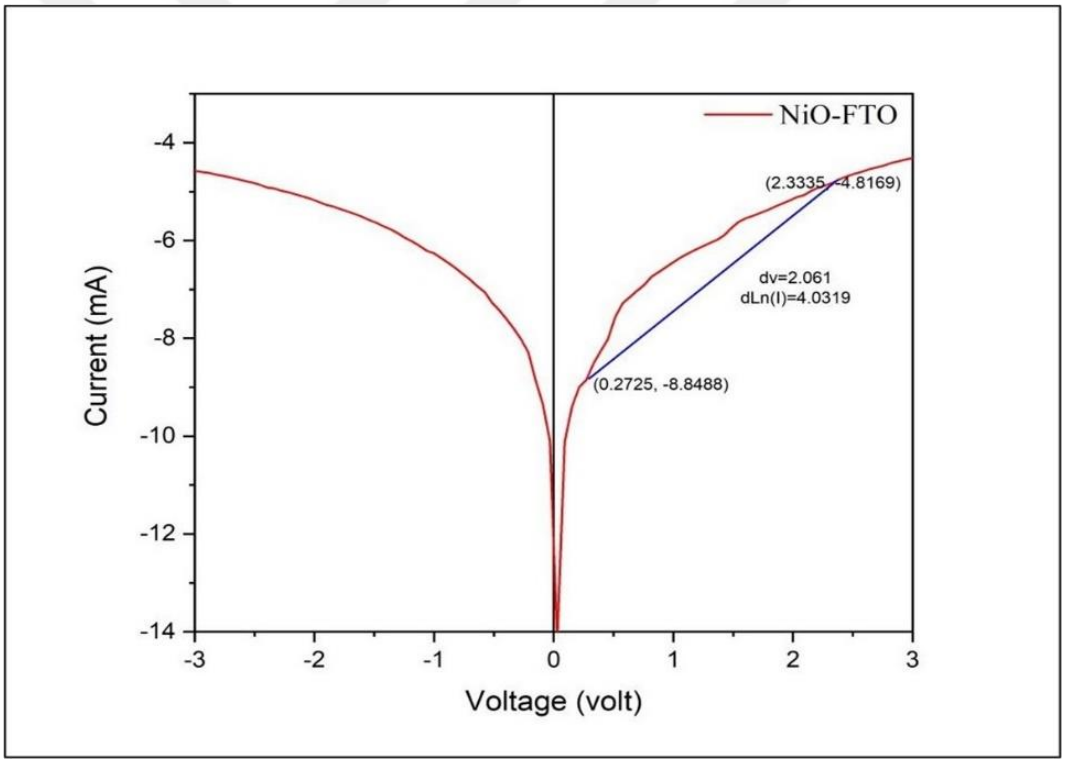

Figure 0.7 The log I-V plots of (NiO-FTO)

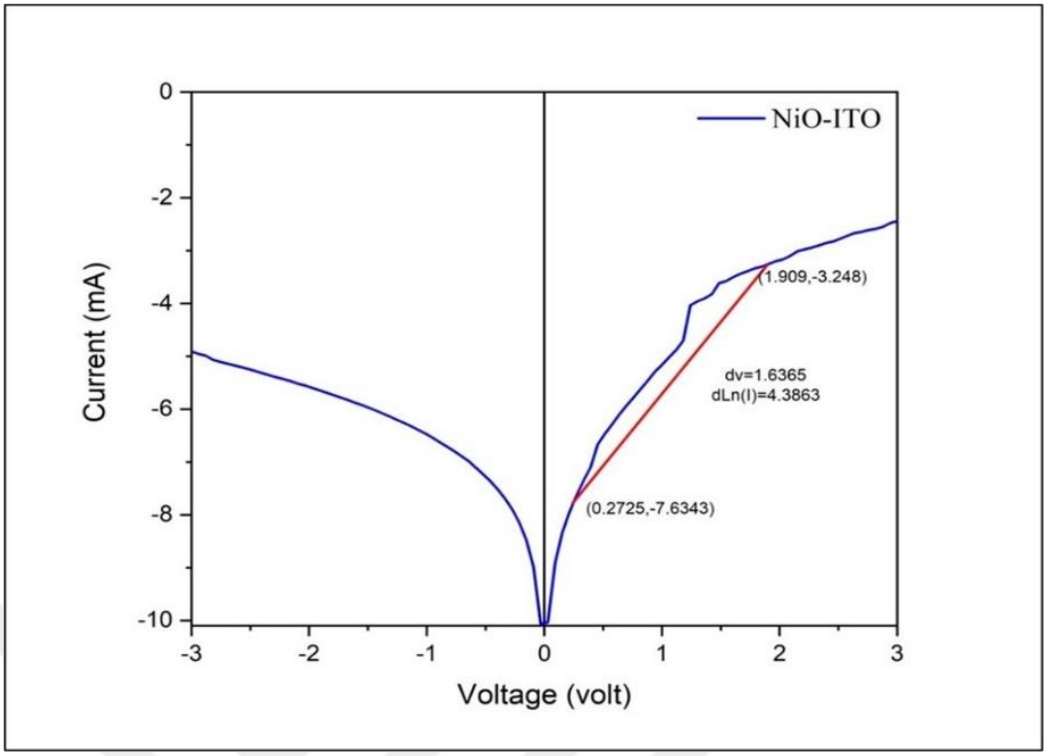

Figure 0.8 The log I-V plots of (NiO-ITO)

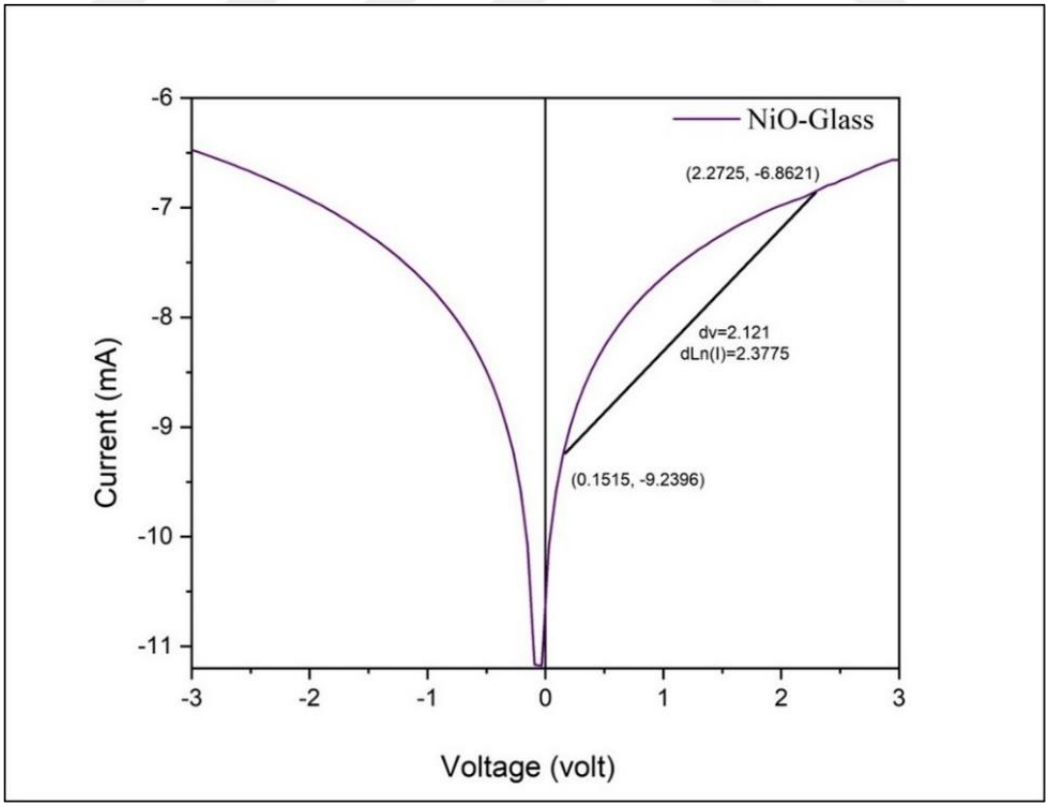

Figure 0.9 The log I-V plots of (NiO-GLASS)

5. CONCLUSION AND RECOMMENDATIONS

In this thesis, NiO films were produced by using different substrates with the SILAR method. The effect of the substrate on the structural, optical, electrical, and surface properties of the films was investigated.

- It was determined that (NiO-ITO) films have higher optical transmittance and higher Urbach energy value than other films.

- The differences in energy levels at the band edge of NiO-ITO films are less. This showed that NiO-ITO films would be more suitable in terms of band structure compatibility.

- NiO-ITO films showed different electrical properties with small saturation current and diode behavior

- The crystal structures of (NiO-ITO) films were found to have greater consistency and smaller crystal size than other films.

- The most homogeneous and round grain surface morphology was observed in NiO-ITO films.

- It has been determined that the use of ITO base in the production of NiO films with the SILAR method will significantly improve the quality of the films and increase the potential of the films to be used in different areas.

- The effect of the film thickness can be determined by storing the films in different thicknesses on the ITO substrate.

- It is possible to change the properties by changing some parameters of the SILAR method (mole ratio of materials, solution temperatures and annealing temperature, number of duty cycles).

- Doping can be done to improve some properties and the effect of the doping element on NiO films can be studied.

- The films have ohmic electrical properties and can be applied in some gas sensors or as a light absorbing layer.

REFERENCES

Abed, O. Z., Kamel, A. A. and Chiad, S. S. 2014. Effect of Thickness on the Structural Parameters of (NiO) Films Prepared by the Chemical Spray Pyrolysis. Diyala Journal For Pure Science, 10: 3-2.

Abdullah, M. A. R., Mamat, M. H., Ismail A. S., Malek M. F., Suriani A. B., Ahmad M. K., Shameem Banu I. B., Amiruddin, R., Rusop, M. 2019. Direct and seedless growth of Nickel Oxide nanosheet architectures on ITO using a novel solution immersion method. Materials Letters, 236: 460-464.

Abuelwafa, A. A., Abd El-sadek, M. S., Elnobi, S. And Soga, T. 2021. Effect of transparent conducting substrates on the structure and optical properties of tin (II) oxide (SnO) thin films: Comparative study. Ceramics International, 47(10), 13510-13518.

Abu-Yaqoub, A. Y. S. 2012. Electrochromic Properties of Sol-gel NiO–based films (Doctoral dissertation).

Adachi, H. , Wasa, K. 2012. Handbook of Sputter Deposition Technology, In: Thin Films and Nanomaterials. Wasa, K. Kanno, I. Kotera, H. (eds), pp. 36-39, Elsevier, Amsterdam.

Afre, R. A., Sharma, N., Sharon, M., Sharon M. 2018. Transparent Conducting Oxide Films For Various Applications: A Review. Reviews on Advanced Materials Science, 53: 79-89.

AL-Jawad, S. M., Sabr, A. S. and Elttayef, A. K. 2016. Doping Effect on Structure, Optical, & Sensing Properties of Nanocrystalline (SnO2) Thin Films Prepared by Chemical Bath Deposition (CBD) Technique. Engineering and Technology Journal, 34(5 Part (B) Scientific).

Antony, A., Nisha, M., Manoj, R., Jayaraj, M. K. 2004. Applied Surface Science, 225: 294.

Aouaj, M. A., Diaz, R., Belayachi, A., Rueda, F. and M. Abd-Lefdil. 2009. Comparative Study of ITO and FTO Thin Films Grown by Spray Pyrolysis. Materials Research Bulletin, 44 (7): 1458–61.

Aydın, E. B. and Sezgintürk M. K. 2017. Indium tin oxide (ITO): A promising material in biosensing technology. Trends and Analytical Chemistry, 97: 309-315.

Balestrieri, M. 2014. Transparent conductive oxides with photon converting properties in view of photovoltaic applications: the cases of rare earth-doped zinc oxide and cerium oxide (Doctoral dissertation, Université de Strasbourg).

Banerjee, A. N. and Chattopadhyay, K. K. 2005. Recent Developments in the Emerging Field of Crystalline P-Type Transparent Conducting Oxide Thin Films. Progress in Crystal Growth and Characterization of Materials, 50 (1–3): 52–105.

Baskaran, S. 2010. Structure and regulation of yeast glycogen synthase (Doctoral dissertation).

Batzill M., Diebold U. 2005. The Surface and Materials Science of Tin Oxide. Progress in the Surface Science, 79: 47–154.

Barir, R. 2018. Caractérisation Spectroscopique des Couches minces d'oxyde de Nikel (NiO) Elaborées par Spray (Doctoral dissertation, Université Kasdi Merbah Ouargla).

Benzarouk, H. 2008. Synthèse d'un Oxyde Transparent Conducteur (OTC) Par Pulvérisation Chimique (ZnO, NiO). Mémoire de Magister, Université Badji Mokhtar Annaba.

Berg, H. C. and Purcell, E. M. 1977. Physics of Chemoreception. Biophysical Journal 20 (2): 193–219.

Beyer, W., Hüpkes, J., Stiebig, H. 2007. Transparent conducting oxide films for thin film silicon Photovoltaics. Thin Solid Films, 516: 147–154.

BIOTAIN, 2023. Web site. http://www.crystal-material.com/Substrate-Materials/FTO-coated-glass-conductive.html. Date of access: 25.04.2023.

Birnie, D. P. 2004. Sol-Gel Technologies for Glass Producers and Users, In: Spin Coating Technique, Aegerter, M. A., Mennig, M. (eds), Spinger, pp. 49-55, Switzerland.

Bushberg, J. T. and Boone, J. M. 2011. The Essential Physics of Medical Imaging. Lippincott Williams & Wilkins, 1048 page, New York.

Caporaletti, O. 1982. Electrical and Optical Properties of Bias Sputtered ZnO Thin Films. Solar Energy Materials, 7 (1): 65–73.

Chang, C. C., Scarr, N. And Kumta, P. N. 1998. Synthesis and Electrochemical Characterization of LiMO2 (M= Ni, Ni0. 75Co0. 25) for Rechargeable Lithium Ion Batteries. Solid State Ionics, 112 (3–4): 329–44.

Chatterjee, Sa. K. 2008. Experimental Methods for Structure Analysis: X-Ray Diffraction Techniques. Crystallography and the World of Symmetry, 1: 57–75.

Chavan G. T., Kim, Y., Khokhar, M. Q., Hussain, S. Q., Cho, E. C., Yi, J., Ahmad, Z., Rosaiah, P., Jeon, C. W. 2023. A Brief Review of Transparent Conducting Oxides (TCO): The Influence of Different Deposition Techniques on the Efficiency of Solar Cells. Nanomaterials, 13(1226): 1-19.

Chavillon, B. 2011. Synthèse et caractérisation d'oxydes transparents conducteurs de type p pour application en cellules solaires à colorant (Doctoral dissertation, Université de Nantes).

Clark I. B. 2007. Review of Transparent Conductive Oxides (TCO). Society of Vacuum Coaters, 1-8.

Cole, J. M. 2004. Single-Crystal X-Ray Diffraction Studies of Photo-Induced Molecular Species. Chemical Society Reviews, 33 (8): 501–13.

Colombel, F., Castel, X., Himdi, M., Legeay, G., Vigneron, S., Cruz, E. M. 2009. Ultrathin metal layer, ITO film and ITO/Cu/ITO multilayer towards transparent antenna. IET Science, Measurement and Technology, 3: 229-234.

Dauzhenka T.A., Ksenevich V.K., Bashmakov I.A., Galibert J. 2011. Origin of Negative Magnetoresistance in Polycrystalline SnO_2 Films. Physics Review B. 83: 165309.

Diao, C. C., Huang, C. Y., Yang, C. F. And Wu, C. C. 2020. Morphological, Optical, and Electrical Properties of p-Type Nickel Oxide Thin Films by Nonvacuum Deposition. Nanomaterials, 10 (4): 636.

Dickinson, W. C. and Cheremisinoff, P. N. 1980. Solar Energy Technology Handbook. Part B-Applications, Systems Design, and Economics, pp. 6, New York.

Elkaiem, A. 2015. Contribution Au Développement Des Matériaux Nano-Composites à Base de ZnO et Polymère Etude Structural et Optique. Material Science, 139337937.

Elangovan, E., Ramamurthi, K. 2005. Studies on micro-structural and electrical properties of spray-deposited fluorine-doped tin oxide thin films from low-cost precursor. Thin Solid Films, 476(2): 231-236.

Ellmer, K. and Klein, A. 2008. ZnO and Its Applications. In Transparent Conductive Zinc Oxide, Springer, pp. 1–33, Berlin.

Fallah, H. R., Ghasemi, M., Hassanzadeh, A. and Steki, H. 2007. The Effect of Annealing on Structural, Electrical and Optical Properties of Nanostructured ITO Films Prepared by e-Beam Evaporation. Materials Research Bulletin, 42 (3): 487–96.

Ferhati, H., Bendjerad, A., Djeffal, F., Benhaya, A., Saidi, A. 2021. Multispectral photodetection using low-cost sputtered NiO/Ag/ITO heterostructure:From design concept to elaboration. Ceramics International, 47: 15703-15709.

Frey, H. and Khan, H. R. 2015. Handbook of Thin Film Technology, Springer, 12 page, Berlin.

Frey, H. and Khan, H. R. 2015. Handbook of Thin Film Technology, Springer, 225 page, Berlin.

Fortunato, E., Ginley, D., Hosono, H. Paine D. C. 2007. Transparent Conducting Oxides for Photovoltaics. MRS Bulletin, 32(3): 242-247.

Elsheikh, Mo. H., Shnawah, D. A., Mohd Sabri, M. F., Mohd Said, S. B., Hassan, M. H., Bashir, M. B. A. And Mohamad, M. 2014. A Review on Thermoelectric Renewable Energy: Principle Parameters That Affect Their Performance. Renewable and Sustainable Energy Reviews, 30: 337–55.

Exarhos, G. J. and Zhou, X. D. 2007. Discovery-Based Design of Transparent Conducting Oxide Films. Thin Solid Films, 515 (18): 7025–52.

Gençyılmaz, O. 2021. Transition Metals (Cu/Co/Mn) Doped NiO Films: Structural, Optical and Morphological Properties. Journal of Materials and Electronic Devices 6 (1): 7–15.

Geremew, T. 2022. Thin Film Deposition and Characterization Techniques. Journal of 3D Printing and Applications, 1(2): 1-24.

Ghasemi, H., Mozaffari, M. H., Moradian, R., Ghobadi, N. 2022. Optical and electrical properties of ITO/Metal/NiO triple-layer grown by PVD method: An

experimental study. Materials Science in Semiconductor Processing, 149: 106853.

Granqvist, C. G.. Hultåker, A. 2002. Transparent and conducting ITO films: New developments and applications. Thin Solid Films, 411: 1–5.

Gross C. A. and Roppel T. A. 1996. Fundamentals of Electrical Engineering, CRC Publishing, 352 page, New York.

Hamilton, D. J. 2003. On the Influence of Surface Treatment on Electrical Characteristics of Schottky Diodes. Journal of the Microelectronic Engineering Conference, 13: 5.

Haacke, G. 1976. New figure of merit for transparent conductors. Journal of Applied Physics, 47: 4086–4089.

Hecht, D. S., Liangbing, H., Irvin, G. 2011. Emerging Transparent Electrodes Based on Thin Films of Carbon Nanotubes, Graphene, and Metallic Nanostructures. Advanced Materials, 23 (13): 1482–1513.

Hedges, J. I. and Oades, J. M. 1997. Comparative Organic Geochemistries of Soils and Marine Sediments. Organic Geochemistry, 27 (7–8): 319–61.

Hiramatsu, H., Kamiya, T., Tohei, T., Ikenaga, E., Mizoguchi, T., Ikuhara, Y., Kobayashi, K., Hosono, H. 2010. Origins of hole doping and relevant optoelectronic properties of wide gap p-type semiconductor, lacuose. Journal of Chemical Society - Chemistry Science Journals, 132: 15060-15067.

Holzhey, P., Prettl, M., Collavini, S., Mortan, C., Saliba, M. 2023. Understanding the impact of surface roughness: changing from FTO to ITO to PEN/ITO for fexible perovskite solar cells. Scientifc Reports, 13: 6375-3681.

Hu, Z., Zhang, J., Hao, Z., Hao, Q., Geng, X. and Zhao, Y. 2011. Highly Efficient Organic Photovoltaic Devices Using F-Doped SnO_2 Anodes. Applied Physics Letters, 98 (12): 66.

Hudaya C., Jeon B.J., Lee J. K. 2015. High Thermal Performance of SnO_2:F Thin Transparent Heaters with Scattered Metal Nanodots. ACS Applied Material Interfaces, 7: 57–61.

Jang, J., Kang, Y., Cha, D., Bae, J., Lee, S. 2019. Thin-Film Optical Devices Based on Transparent Conducting Oxides: Physical Mechanisms and Applications. Crystals, 9(4): 192-204.

Jaya, R. P. 2020. New Materials in Civil Engineering, In:Porous concrete pavement containing nanosilica from black rice husk ash. Samui, P. (ed), Elsevier Publishing, pp. 493-527, Amsterdam.

Kaleli, M., Aldemir, D. A., Bayram, A. B., Yavru, C. A. 2019. Structural, Morphological, Optical and Electrical Analysis of Fluorine Doped Tin Oxide Thin Films Fabricated by Ultrasonic Spray Pyrolysis. Düzce University Journal of Science and Technology, 7: 2107-2115.

Kalyani, N. T. and Dhoble, S. J. 2012. Organic Light Emitting Diodes: Energy Saving Lighting Technology A Review. Renewable and Sustainable Energy Reviews, 16 (5): 2696–2723.

Kasap, S. O. 2006. Principles of Electronic Materials and Devices. McGraw-Hill, vol. 2, New York.

Kawashima, T., Matsui, H., Tanabe, N. 2003. New transparent conductive films: FTO coated ITO. Thin Solid Films, 445: 241–24.

Khalifa, K.. 2015. Structural and Opto-Electrical Study of SnO2 Thin Films Elaborated by Spray Pyrolysis (Home Made). Applied Physics Radiation and Energy, MSc. Thesis, University of El-oued Faculty of Sciences and Technology, 73 page, Algeria.

Kim, D. H. , Park M. R. , Lee H. J. , Lee G. H. 2006. Thickness dependence of electrical properties of ITO film deposited on a plastic substrate by RF magnetron sputtering. Applied Surface Science, 253: 409-411.

Kittel, C. 2004. Introduction to Solid State Physics, John Wiley and Sons Publishing, 396 page, New York.

Kohli, R. 2012. Detection, Characterization, and Analysis of Contaminants, In: Developments in Imaging and Analysis Techniques for Micro- and Nanosize Particles and Surface Features. Kohli, R. and Mittal K. L. (eds), Elsevier, pp. 215-306, Amsterdam.

Kwak, D. J., Moon, B. H., Lee, D. K., Park, C. S., Sung, Y. M. 2011. Comparison of transparent conductive indium tin oxide, titanium-doped indium oxide, and fluorine-doped tin oxide films for dye-sensitized solar cell application. Journal of Electrical Engineering and Technology, 6(5): 684-687.

Li, F., Chong C., Furui T., Chunxi L., Yue, G., Shen, L. And Zhang, W. 2014. Semitransparent Inverted Polymer Solar Cells Employing a Sol-Gel-Derived TiO_2 Electron-Selective Layer on FTO and MoO_3/Ag/MoO_3 Transparent Electrode. Nanoscale Research Letters, 9 (1): 1–5.

Liu, D. C., Aragaw, B. A., Shi, J. B., Lee, M. W. 2017. $PbBi_4S_7$: A New Infrared Solar Absorber Material Exhibiting High Photocurrents. Journal of Electrochemical Society 164: F804–F808.

Lopez, C. 2003. Materials Aspects of Photonic Crystals. Advanced Materials, 15 (20): 1679–1704.

Macdonald, J. R. 1953. Theory of Ac Space-Charge Polarization Effects in Photoconductors, Semiconductors, and Electrolytes. Physical Review, 92 (1): 4-17.

Manthrammel, M. A., Shkir, M., Ganesh, V., Khan, A., AlFaify, S. 2020. Facilely fabricated Sr@NiO/FTO films and their characterizations for opto-nonlinear applications. Chinese Journal of Physics, 66: 91-101.

Mesrouk, M. 2013. Etude d'une électrode tri-couches à base de TCO/Métal/TCO pour une céllule solaire organique (Doctoral dissertation, Université Mouloud Mammeri).

Miccoli, I., Edler, F., Pfnür, H., Tegenkamp, C. 2015. The 100th anniversary of the four-point probe technique: the role of probe geometries in isotropic and anisotropic systems Journal of Physics: Condensed Matter, 27(223201): 1-29.

Minami T. 2005. Transparent conducting oxide semiconductors for transparent electrodes. Semiconductor Science Technology. 20(4): S35.

Moholkar, A.V., Pawar, S. M., Rajpure, K.Y., Bhosale, C. H. 2007. Effect of solvent ratio on the properties of highly oriented sprayed fluorine-doped tin oxide thin films. Material Letters, 61: 3036-3036.

Napari, M., Huq, T. N., Hoye, R. L. Z. and MacManus Driscoll, J. L. 2021. Nickel Oxide Thin Films Grown by Chemical Deposition Techniques: Potential and Challenges in Next generation Rigid and Flexible Device Applications. InfoMat, 3 (5): 536–76.

Nazarzadehmoafi, M. 2017. Electronic Properties of Metal-In_2O_3 Interfaces. PhD. Thesis, Humboldt University, 175 page, Berlin.

Nguyen, T. T., Dao, K. A., Nguyen, T. T., Nguyen, C. D., Nguyen, S. H., Huong, T. M. 2020. Nguyen Influence of Thermal Annealing Media on Optical and Electrical Properties of FTO, ITO and TiO_2 Films. Materials Transactions, 61(11): 2091-2094.

Nicolau, Y. F. 1985. Solution deposition of thin solid compound films by a successive ionic-layer adsorption and reaction process. Applications of Surface Science, 22(2): 1061-1074.

Noh, S. I., Ahn, H. J., Riu, D.H. 2012. Photovoltaic property dependence of dye-sensitized solar cells on sheet resistance of FTO substrate deposited via spray pyrolysis. Ceramics Intirnational, 38: 3735-3739.

Novoselov, K. S. and Castro Neto, A. H. 2012. Two-Dimensional Crystals-Based Heterostructures: Materials with Tailored Properties. Physica Scripta, 2012 (T146): 014006.

NTFL Your Coating Solution, 2023. Web site. https://newportlab.com/ito/ Date of access: 25.04.2023.

Padvi, M. N., Moholkar, A., Prasad, S. R. And Prasad, N. R. 2021. A Critical Review on Design and Development of Gas Sensing Materials. Engineered Science, 15: 20–37.

Pankove, J. I. and Carlson, D. E. 1976. Electroluminescence in Amorphous Silicon. Applied Physics Letters, 29 (9): 620–22.

Pathan, H. M. and Lokhande C. D. 2004. Deposition of metal chalcogenide thin films by successive ionic layer adsorption and reaction (SILAR) method Bulletin Material Science, 27: 85-111.

Patil, P. S. and Kadam, L. D. 2002. Preparation and Characterization of Spray Pyrolyzed Nickel Oxide (NiO) Thin Films. Applied Surface Science, 199 (1–4): 211–21.

Pissadakis, S., Mallis, S., Reekie, L., Wikinson, J. S., Eason, R. W., Vainos, N. A., Moschovis, K., Kiriakidis, G. 1999. Applied Physics A 69: 333-336.

Plá Cid C. C., Spada E. R., Sartorelli M. L. 2013. Effect of the cathodic polarization on structural and morphological proprieties of FTO and ITO thin films. Applied Surface Science 273: 603–606.

Pulker, H. K. 2019. Film Production Methods in Precision Optics, Springer, 353 page, Berlin.

Raebiger, H., Lany, S., Zunger, A. 2007. Origins of the p-type nature and cation deficiency in Cu_2O and related materials. Phys. Rev. B 76: 045209.

Rakibuddin, M., Shinde, M. A., Kim H. 2020. Sol-gel fabrication of NiO and NiO/WO_3 based electrochromic device on ITO and flexible substrate. Ceramics International, 46: 8631-8639.

Rahal, A. 2013. Elaboration Des Verres Conducteurs Par Déposition de ZnO Sur Des Verres Ordinaires. MSc. Thesis, Unıversıty of D'Eloued, 94 page, Algeria.

Rödl, C., Schleife, A. 2014. Photoemission spectra and effective masses of n-and p-type oxide semiconductors from first principles: ZnO, CdO, SnO2, MnO, NiO. Physics Status Solidi A, 211: 74–81.

Sauter, D., Weimar, U., Noetzel, G., Mitrovics, J., Göpel, W. 2000. Development of modular ozone sensor system for application in practical use. Sensor Actuators B, 69: 1–9.

Smart, L. E. and Moore, E. A. 2012. Solid State Chemistry: An Introduction. CRC press, 507 page, New York.

Sokolik, I., Andronova, A. and Johnson, T. C. 1993. Complex Refractive Index of Atmospheric Dust Aerosols. Atmospheric Environment. Part A. General Topics, 27 (16): 2495–2502.

Søndergaard, R. R., Hösel, M. and Krebs, F. C. 2013. Roll-to-Roll fabrication of large area functional organic materials. Journal of Polymer Science Part B: Polymer Physics, 51(1), 16-34.

Sullivan, I., Zoellner, B. and Maggard, P. A. 2016. Copper (I)-Based p-Type Oxides for Photoelectrochemical and Photovoltaic Solar Energy Conversion. Chemistry of Materials, 28 (17): 5999–6016.

Sze, S. M. 1981. Physics of Semiconductor Devices, John Wiley and Sons Publishig, 12 page, New York.

Sze, S. M., Li, Y. and Kwok, K. N. 2021. Physics of Semiconductor Devices. John wiley & sons, 994 page, New York.

Taşköprü, T., Turan, E., Zor, M. 2016. Characterization of NiO films deposited by homemade spin coater. International Hydrogen Energy, 41: 6965-6971.

Qu, W., Wlodarski, W., Meyer, J. U. 2000. Comparative Study on Micromorphology and Humidity Sensitive Properties of Thin-Film and Thick-Film Humidity Sensors Based on Semiconducting $MnWO_4$. Sensors and Actuators B: Chemical, 64 (1–3): 76–82.

Vander Kam, S. K., Gawalt, E.S., Schwartz, J., Bocarsly, A. B. 1999. Electrochemically active surface zirconium complexes on indium tin oxide. Langmuir 15: 6598–6600.

Waremra, R. S. and Betaubun, P. 2018. Analysis of Electrical Properties Using the Four Point Probe Method. In E3S Web of Conferences, 73: 13019.

Wu S., Yuan S., Shi L., Zhao Y., Fang J. 2010. Preparation, Characterization and Electrical Properties of fluorine-Doped Tin Dioxide Nanocrystals. Journal of Colloid Interface Science, 346: 12–16.

Yang G. W. 2007. Laser ablation in liquids: Applications in the synthesis of nanocrystals. Progress in Materials Science, 52: 648-698.

Yang, J., Yu, X., Li, Y., Cheng, G., Yi, Z., Zhang, Z., Chi, F., Liu, L. 2022. A Novel Dye-Sensitized Solar Cell Structure Based on Metal Photoanode without FTO/ITO. Micromachines, 13: 122-132.

Yaseen, M., Cowsill, B. J., Lu,J. R. 2012. Coating for Biomedical Applications, In: Characterisation of biomedical coatings. Driver, M. (ed), Woodhead Publishing, pp. 176-220, Amsterdam.

Young, D. J. 2008. High Temperature Oxidation and Corrosion of Metals. Elsevier, 592 page, New York.

Zakutayev, A. McIntyre, D., Schneider, G., Kykyneshi, R., Keszler, D., Park, C. H., Tate, J. 2010. Tunable properties of wide-band gap p-type bacu $(Ch_{1-x}Ch_x')F$ (Ch = S, Se, Te) thin-film solid solutions. Thin Solid Films, 518: 5494–5500.

Zayim E. Ö., Turhan, I., Tepehan, F. Z., Özer, N. 2008. Sol–gel deposited nickel oxide films for electrochromic applications. Solar Energy Materials & Solar Cells, 92: 164-169.

Zhang, S. 2017. Study of fluorine-doped tin oxide (FTO) thin films for photovoltaics applications. PhD. Thesis, Université Grenoble Alpes, 225 page, France.

Zhang, Y., Holzwarth, N. A. W., Williams, R. T. 1998. Electronic Band Structures of the Scheelite Materials $CaMoO_4$, $CaWO_4$, $PbMoO_4$, and $PbWO_4$. Physical Review B, 57 (20): 12738.